PHOTOEXCITED HYPERSONIC SURFACE ACOUSTIC WAVES PROPAGATING UNDER PERIODIC METAL GRATING

BY

JYOTHI SWAROOP SADHU

THESIS

Submitted in partial fulfillment of the requirements
for the degree of Master of Science in Mechanical Engineering
in the Graduate College of the
University of Illinois at Urbana-Champaign, 2010

Urbana, Illinois

Adviser:

Dr. Sanjiv Sinha

ABSTRACT

Photoinduced strain gradients in nanometer length scales using periodically patterned grating on a substrate is an attractive way of producing coherent surface acoustic waves (SAW). Ultrafast laser pulses incident on this structure produce constrasting thermal strain in the grating and the substrate thus launching surface acoustic waves. The frequency of the SAW is inversely dependant on the period of the grating and thus the generation of high frequency SAW (ν ~1-100 GHz) requires sub-micron scale gratings. Hypersonic SAW are scientifically significant for photoacoustic spectroscopy and metrology of nanostructures in addition to investigations of phonon mediated heat transport.

In this work, we study the propagation of hypersonic surface acoustic waves (ν ~10-20 GHz) in silicon with aluminum gratings fabricated on them for varying periods and duty cycles (η) of the grating (coverage ratio of Al on Si). Modeling the optical absorption of the laser and the resultant thermoelastic strain reveals requirements on the elastic and the thermal properties of the grating and the substrate for efficient SAW generation. Using the time resolved reflectivity measurements, we show that the SAW frequency shift $\Delta\nu$ with the duty cycle departs from the widely used perturbation theory by $sin^2(\pi\eta)$ with highest deviation around $\eta = 0.5$. A similar finding for attenuation of SAW suggests that mass loading on SAW by Al grating places limitation on the duty cycle in design of hypersonic phononic crystals. Further, we conduct finite element based eigenmode analysis on the Si-Al periodic composite which show a good agreement with the experimental data. Modal analysis further reveals that higher attenuation in the duty cycle regime $\eta = 0.3 - 0.6$ is due to radiation of the energy from the surface modes into the bulk due to mass loading from the Al grating.

ACKNOWLEDGMENTS

I wish to express my gratitude to my advisor Dr. Sanjiv Sinha, firstly for agreeing to supervise my research and guiding me through several bottlenecks I faced during the course of my research work. I am extremely thankful to Prof Sinha for dedicating time in explaining the fundamentals required for my research as I entered as a novice into this field.

Special acknowlegdements to my collaborator in this project J. H. Lee whose help was instrumental in setting up the experiments. I would also extend sincere thanks to my research group, O. T. Baris and T. Hongxiang for critical discussion of the results throughout the project. Last but not least, I would like to thank Marc Ghossoub for insightful comments on the research and his patience in troubleshooting experimental malfunctions. Outside my research group, I would like to thank L. Nishanth and Dr. Sambit Mishra for their valuable suggestions on the literature required for my project.

TABLE OF CONTENTS

LIST OF FIGURES v

LIST OF ABBREVIATIONS viii

CHAPTER 1 INTRODUCTION 1
1.1 Structure of the Thesis 6

CHAPTER 2 THEORY OF PHOTOEXCITED SURFACE WAVES . 7
2.1 Theory 8
2.2 Opto-Acoustic Generation 11
2.3 Analysis of SAW field 14
2.4 Damping of SAW waves 17
2.5 Conclusion 17

CHAPTER 3 EXPERIMENTAL RESULTS 19
3.1 Introduction 19
3.2 Fabrication 20
3.3 Picosecond Ultrasonics 20
3.4 Acoustic Signals from TDTR data 22
3.5 Duty cycle effect on SAW characteristics 24

CHAPTER 4 MODAL ANALYSIS OF PHONONIC CRYSTALS . . 31
4.1 Modeling of unit cell of periodic composite 31
4.2 Analysis of surface modes with duty cycle 34
4.3 Attenuation with the duty cycle 38

CHAPTER 5 SUMMARY AND CONCLUSIONS 42

REFERENCES 45

LIST OF FIGURES

1.1 The frequency map showing THz regime and THz electromagnetic sources. 2
1.2 (a) Periodic gratings on substrate (b) Optical Interferometry (ISTS) (c) PDMS mask with substrate in near field. . . . 4
1.3 Grating assisted interaction of SAW and BAW in a substrate. 5

2.1 Laser radiated onto the grating structure on a substrate. The substrate is modeled as a semi-infinite homogeneous medium with z=0 coinciding with the surface of the substrate. 9
2.2 (a) **MHz-GHz range:** The thermal wavelength is insignificant in comparison to that of acoustic wavelength at lower frequencies of SAW (b) **Beyond GHz:** The thermal and acoustic wavelengths are comparable for frequencies above 10 GHz. 13
2.3 (a) Frequency Dependence of $\tilde{F}_t(\omega)$ with variation in rise time of pulse. The plot shows that the frequency contribution by the factor $\tilde{F}_t$ increases as the length of the pulse shortens. (b) Effect on $F_z(\omega)$ with increasing absorption coefficients at k=10 W/m/K. (c) Spectral Dependence of the F_r(r) shows that the decrease in period of grating leads to higher frequency components of SAW. 15
2.4 This graph shows the summary of the frequency dependance of the the three functions and the parameters influencing them. The resultant SAW is the product of the three curves here. In this figure, t_0=100fs rise time laser incident on high absorbing substrate ($\alpha = 5 \times 10^6 m^{-1}$) with spatial period p=100 nm. 16

3.1 (a) The Al lines on Si are patterned by e-beam lithography followed by Al deposition and lift off steps. (b) The SEM images of the samples showing the period of gratings. 21
3.2 (a) The pump beam heats up the Al lines by over 100 K. The heat is eventually dissipated through Al-Si interface (b) The probe beam monitors the strain induced reflectance change of surface in time. 21

3.3 The optical circuit for TDTR experiment is shown. Both pump and probe focused onto the sample have a time delay controlled by mechanical stage. 22
3.4 (a) The typical TDTR signals showing acoustic oscillations and decay in temperature. (b) The acoustic signal extracted from TDTR signal by removing thermal background. 23
3.5 The power spectrum of TDTR signal for 300 nm grating without thermal background. 24
3.6 The power spectrum of acoustic signals for 300 nm and 400 nm grating. 25
3.7 The acoustic signals and their corresponding transforms for 400 nm gratings at different duty cycles is shown. 25
3.8 The experimental sample description with the peak SAW frequency and damping time is tabulated. (The samples with * have higher scale of roughness on Al lines. 26
3.9 The frequency dispersion with the duty cycle is grating for 400 nm gratings. Also shown is the prediction by perturbation theory. 27
3.10 The SAW velocity dispersion with the duty cycle is grating for 400 nm and 300 nm gratings. The unperturbed velocity of SAW in Si is 4910 m/s. 28
3.11 The acoustic signal is fitted by a synthetic waveform to obtain attenuation of the wave. 29
3.12 The lifetime of surface oscillations plotted against duty cycle for 400 nm and 300 nm gratings. 30

4.1 The unit cell of the periodic composite with a width equals wavelength of the modes to be analyzed. 32
4.2 Fine mesh at the surface. 33
4.3 The displacement pattern of a Rayleigh mode. 33
4.4 Rayleigh mode on free Si surface with two polarizations (a) and (b). 34
4.5 In the high duty cycle regime, $\Delta\nu$ follows a linear downward shift. The displacement fields show that energy is only concentrated near the surface. 35
4.6 In this regime, $\Delta\nu$ follows sinusoidal trend and shows highest deviation from perturbation theory. The displacement fields show significant coupling of surface modes with the bulk. 36
4.7 In this regime, $\Delta\nu$ becomes more linear and creeps towards perturbation theory below $\eta = 0.2$. 37
4.8 The frequencies obtained by full eigenmode analysis have excellent agreement with experiment for 300 nm and 400 nm gratings. 37

4.9 (a) The frequencies obtained by full eigenmode analysis have excellent agreement with experiment for 300 nm and 400 nm gratings. 38
4.10 (a) The spread of E_{distr} around peak frequency increases from $\eta = 0.9$ to $\eta = 0.7$. 39
4.11 (a) The lifetime of surface oscillations predicted by eigenmode analysis for 300 nm and 400 nm has good match with experimental data. 40

5.1 (a) The experimental SAW velocity shift (on left) and the frequencies of excited surface waves for $p = 400$ nm (on right) show good agreement with the results obtained by eigenmode analysis of the unit cell of the structure (shown in inset). The thin film perturbation theory is only valid for $\eta < 0.2$ (region (I)). (b) The displacement fields of the excited mode in different duty cycle regimes show highest coupling of surface modes with bulk modes in region (II). . . . 44
5.2 The damping time (γ) of surface acoustic waves in $p = 400$ nm is shown on the right of axis at corresponding cycles (square dots). The plot of damping time normalized by square of period (on left) as a function of duty cycle shows the highest attenuation in region(II). The damping time obtained by taking inverse of FWHM of surface energy spread ($0 < z < p$) around SAW mode is also shown. 44

LIST OF ABBREVIATIONS

SAW	Surface Acoustic Waves
FWHM	Full Width Half Maximum
TDTR	Time-Domain Thermoreflectance
ISTS	Impulsive Stimulated Thermal Scattering
BAW	Bulk acoustic waves
TPF	Transition point frequency

CHAPTER 1

INTRODUCTION

High frequency acoustics serve as a novel tool for characterizing the mechanical properties of materials in addition to controlling the fundamental physical processes like heat and electron transport. Many acoustic wave devices have found their applications in varied scientific fields, mainly as sensors by using different polarizations of sound like bulk acoustic wave (BAW), Love surface acoustic waves (LSAW), shear horizantal waves (SHW), Rayleigh surface waves and Lamb waves. As each acoustic wave device has their distinct advantage, the surface acoustic waves (SAW) have been of special interest due to the confinement of elastic energy near the surface rendering the wave to be sensible to even the slightest perturbation on the surface. This property of SAW is utilized in chemical, biological, temperature and gravimetric sensors to name a few. SAW devices are extensively used in electronic industry for construction of delay lines where SAW on piezo substrates is transduced to electrical signals using interdigitated transducers.

The utility of SAW can be extended to nanoscale applications ranging from sensing to communications by increasing their frequencies to hypersonic regime (ν $\sim$1-100 GHz) and beyond. The penetration depth of a surface acoustic wave is in orders of its wavelength. In hypersonic regime, confinement of SAW within sub-100 nm from the surface gives additional advantages in terms of augmented sensitivity and ability to understand surface based physics. Further, research in near terahertz technology and the devices exploiting this frequency band are receiving increasing attention with recent advances in photonics and nanotechnology [1, 2]. Generation of terahertz electromagnetic radiation, referred to as frequencies from 100 GHz-30 THz has been practically realized by various THz sources including femtosecond lasers. The THz technology is growing rapidly with its applications ranging from high speed communications to biosensing [2, 3]. With such potential in

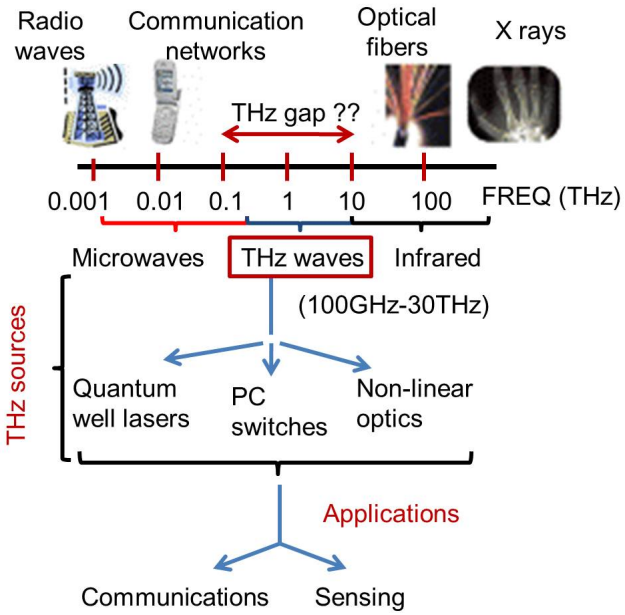

Figure 1.1: The frequency map showing THz regime and THz electromagnetic sources.

sight, the possibility of terahertz surface acoustic devices is technologically significant as the interaction of such high frequency acoustic waves with matter provide new insights into the nanoscale physics and ultrafast dynamics in material systems. Fig 1.1 shows the map of frequency regimes and existing applications of the wavebands.

Piezo based SAW generation is not an attractive option for high frequency SAW generation due to the limited availability of material systems and crystal orientations. Picosecond ultrasonics enables efficient generation of surface acoustic waves (SAWs) through thermo-optic excitation and further, it can also detect the resulting SAW . In this technique, an intense, sub-picosecond laser pulse(pump beam) is absorbed at the surface of the sample. This induces thermal stress in the sample which relaxes by launching an acoustic strain pulse that is detected by another laser pulse (probe beam) by monitoring the strain-induced changes in the reflectivity [4, 5]. Optoacoustic ultrasonics not only enables the use of non-piezoelectrics for SAW sensors but also has a potential to increase the operating frequencies beyond the MHz range of today's SAW sensors to higher GHz and above, enabling applications

spanning microelectronics, microfludics, and non destructive testing [6, 7].

Due to the fact that the hypersonic SAW penetrate the material only upto the wavelength of the wave, hypersonic surface acoustic waves has enabled the study of micromechanical properties of ultrathin film coatings like the elastic constants by estimating the sound velocities [5]. This surface confinement of SAW enable them to be very sensitive towards any changes occurring on the substrate surface. High frequenc SAW have the ability to sense mass variations in range of femtograms thus enabling study of biomolecule bonding [3]. The hypersonic and near THz regime of SAW increases the processing speed of SAW sensors in communications technology potentially enabling ultrafast wireless communications. In addition, photoacoustic spectroscopy remains a topic of continuing interest owing to its ability to characterize ultrafast carrier dynamics in material systems with nanometer length scales which enhances the studies of coherent control of phonons [8], phonon focusing [9], single electron transport in 1D channels [10] and ballistic phonon transport [6, 11, 12].

In picosecond ultrasonics, there are various principles of generating surface acoustic wave. The first technique called impulsive stimulated thermal scattering (ISTS) or transient grating (TG) method (Fig 1.2(b)) uses two or more excitation laser pulses that interfere at the surface of the sample [7]. The interference pattern of these excitation pulses absorbed by the sample defines the periodic thermal field at the surface of the sample. This thermal strain leads to production of counter-propagating surface acoustic waves. The frequency of the surface acoustic waves generated by this technique is given by $\nu = 2V_R sin(\theta/2)/\lambda_e$ where V_R is the Rayleigh velocity of the substrate (=4910 m/s for silicon), θ is the angle of crossing of the excitation pulses while λ_e is their optical wavelength. Thus the SAW frequency that can be generated by this method is limited by the optical wavelength of interfering laser pulses. Extreme ultravoilet to x-rays should be used to increase the SAW frequency. Another technique involves producing the periodic thermal strain in the sample by irradiating laser pulse on a periodic PDMS mask with the sample placed in optical near field as shown in Fig 1.2(c). Finite element based solution of Maxwell equations for this system shows that the near field periodic intensity profile of sub 100 nm periods can only be acheived by ra-

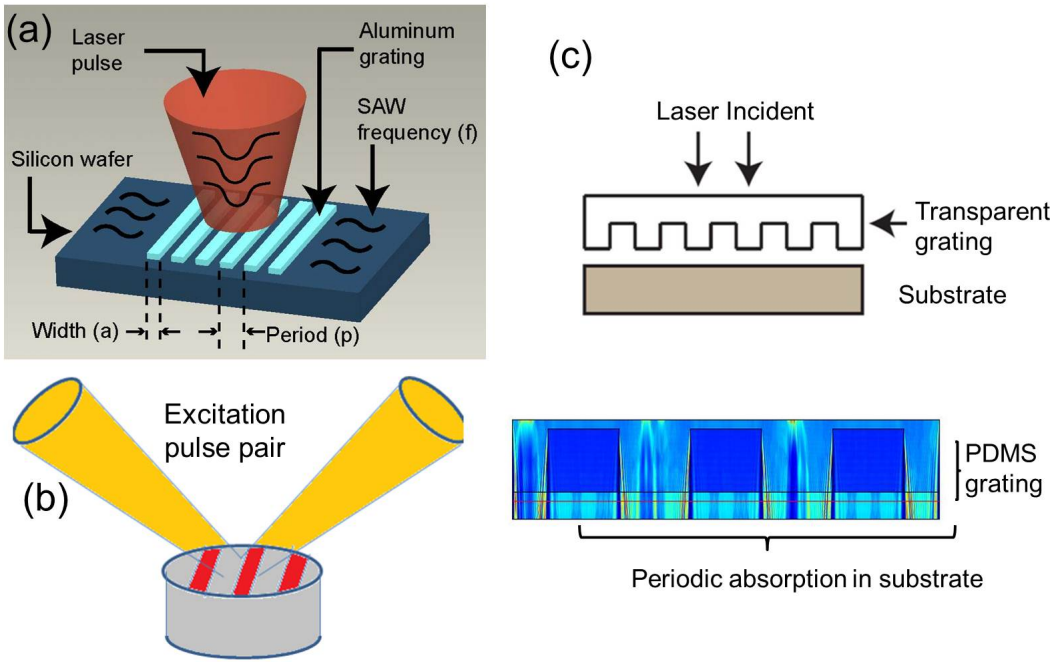

Figure 1.2: (a) Periodic gratings on substrate (b) Optical Interferometry (ISTS) (c) PDMS mask with substrate in near field.

diating x-ray lasers on sub-100 nm patterned PDMS mask.

Generation of the surface acoustic waves using periodically patterned grating directly fabricated onto a substrate as shown in Fig 1.2(a) is attractive way as the frequency of SAW generated using this technique is inversely related to the period of the grating. With advances in nanolithography, feature sizes as small as 50 nm can be fabricated and thus potentially leading to frequencies above 50 GHz [13]. The mechanism responsible for acoustic phonon generation involves coupling between a laser-induced temperature gradient and strain, governed by lattice anharmonicity and can be solved for using the theory of thermoelasticity. Picosecond generation and detection of hypersonic surface acoustic waves (SAW) ($\nu \sim 1 - 50$ GHz) using metal gratings on transparent and semi-transparent substrates is well established in the literature[14, 15, 16, 13]. Such high frequency surface phonons can find potential applications in photoacoustic spectroscopy and the metrology of nanostructures. Hypersonic frequencies generated by this method have been applied in thin film characterization[5], ultrafast actuation of microfluidic channels [17] and for studying phonon [12] and electron transport[10].

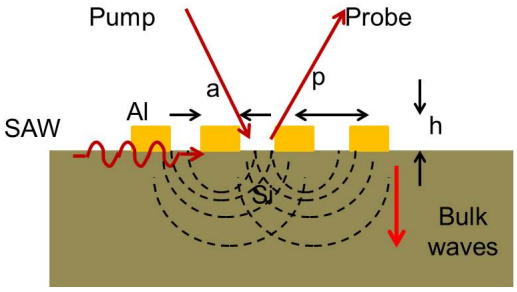

Figure 1.3: Grating assisted interaction of SAW and BAW in a substrate.

However, the SAW generation using this technique has a significant limitation at shorter periods where higher surface confinement of the SAW leads to increased mass loading from the grating suppressing the lifetime of surface vibrations.

The shorter grating periods introduce increased frequency dispersion and attenuation. The presence of the metal grating gives rise to a non-zero stress at the surface of the substrate as the grating is forced to move along with the substrate. This non zero stress causes radiation of energy from the surface vibrations as bulk waves. This effect can be formally described using a perturbation theory [14, 15, 18, 19] which shows that the power density leaked from the SAW to the bulk is inversely proportional to the fourth power of the period of the grating and proportional to the square of the density of the metal grating. The mass loading results in a poor quality factor ($\sim$10), severely limiting applications in high frequency regime. Low density metal gratings like Al are needed to minimize the mass loading since the experiments with dense gratings like gold showed complete suppression of SAW due to heavy mass loading [14].

While there are numerous experiments at hypersonic frequencies on mass loading as a function of period of the metal grating, the effect of the other important parameter, the metal coverage ratio, is relatively unexplored. The dut cycle is defined as the ratio of width of Al and the period of the grating ($\eta = a/p$ from Fig 1.2(a)). In this work, we experimentally study the effect of duty cycle on mass loading using a picosecond acoustics setup. Our focus is on theoretical understanding of SAW generation due to periodic thermal

field using thermoelasticity theory and then understand the limitations of frequencies that can be obtained by using nanostructured grating on the substrate. The results of this work not only gives insight into the design parameters of high frequency surface based phononic crystals but also provides explanation for the physics behind SAW generation.

1.1 Structure of the Thesis

Rest of the thesis is organized in the following manner.

In Chapter 2, a theoretical formulation of surface acoustic wave generation due to photoexcitation of the periodic grating on substrate is presented. The design parameters of the grating and the substrate properties are outlined for high frequency generation. This analysis does not take into account any dissipative mechanisms of the SAW.

In Chapter 3, the experimental results for SAW characteristics in aluminum on silicon structure at different duty cycles and grating periods is presented. The purpose of this study is to understand the extent of mass loading on hypersonic SAW ($\nu \sim$10-20 GHz) due to periodic Al overlay and thus analyze the limitations on SAW frequency in photoexcited phononic crystals.

In Chapter 4, finite element based full eigenmode analysis of the Si-Al periodic composite is presented and show the agreement of the simulation results with the experimental data from Chapter 3. The frequency shift and the attenuation of SAW caused by presence of Al grating at different duty cycles and grating periods are analyzed.

Finally, in Chapter 5, the summary of the experimental and the simulation results from Chapter 3 and Chapter 4 is presented and the conclusions of these results on the design parameters to be controlled for potential generation of higher SAW frequencies are given.

CHAPTER 2

THEORY OF PHOTOEXCITED SURFACE WAVES

In this chapter, the photoacoustic generation of SAW in periodic composites (nano-grating over a substrate) is analyzed using the theories of optical absorption and thermoelasticity. The efficiency of the surface wave generated in this technique is strongly dependant on the choice of substrate and grating material as their contrast in optical, thermal and elastic properties is critical in the generation process. In the theoretical model presented in this chapter, we assume that the mechanical excitation of surface acoustic waves happens only in substrate for a sub-100 nm height metallic overlay which is used for grating. Thus the results only consider elastic properties of substrate and the thermal properties of both the grating and substrate. However, there is a significant perturbation in excited SAW frequencies by interaction of waves in substrate with the metallic overlay and this pertubation depends on the constrast in density and elastic properties of the grating and the substrate. The detailed treatment of mechanical excitation of the waves is considered in Chap 4, while this chapter focuses on how optical field transduces into thermal field and thereby causing thermal strain in substrate that launches the SAW. The design parameters for photoexcitation of hypersonic to near THz surface acoustic waves($1 - 100$ GHz) like laser spot radius, laser pulse time, elastic and thermal properties of the medium are provided by this analysis.

When sub-picosecond laser train pulses are radiated onto a periodic structure, a periodic temperature field is generated along the surface of the substrate due to the differential absorption of radiation along the surface due to grating, that enables the generation of high frequency surface waves. A theoretical model involving optical absorption, thermal diffusion and thermoelastic excitation of waves will yield the information about the parameters to be tailored to control the frequency and the amplitude of surface waves. The laser is modeled by taking into account the Gaussian spatial profile of

Q-switched lasers and the thermal properties of the substrate. Although, the thermoelasticity theory of SAW waves is mature, there have been few attempts at [20, 21] developing a formulation for general intensity profiles. The existing formulations consider frequencies below the GHz, and ignore thermal effects since the acoustic wavelength remains large compared to the thermal wavelength at these frequencies. In this work, we show that this assumption become invalid in the higher GHz range. The validity of the model fails for frequencies above 0.5THz since the wavelength of the surface acoustic waves is comparable to the interatomic distances and the assumption of continuum becomes questionable.

We organize the discussion in this chapter as follows. In section 2.1 , the spectral form of a surface acoustic wave for a general surface temperature profile is derived using the classical model of thermoelasticity. In section 2.2, the temperature field at the surface of the substrate for the grating-on-substrate model is derived. We analyze the dependance of spectral components of SAW with change in the model parameters in section 2.3. This is followed by a discussion on the issues and challenges to generate the near-THz acoustic waves in section 2.4.

2.1 Theory

The generation of surface acoustic waves relies on absorption of a spatially periodic intensity profile of the laser beam. In case of periodic nanostructures on a substrate, the constrast in optical and thermal properties of nanostructure and substrate generates a periodic intensity dictated by period of nanostructure. On periodic absorption of the excitation light at the investigating surface, rapid thermal expansion of the sample causes a surface stress that relaxes as a radially propagating surface wave. The constrast in properties of nanostructure and substrate can be either absorbing substrate/reflective grating or transperent substrate/absorbing grating. In case of a transperent substrate, only the nanostructures are impulse heated by laser which undergo thermal expansion.

Hence the key focus in modeling photothermal generation of surface acoustic waves is understanding the periodic expansion of sample for lateral ther-

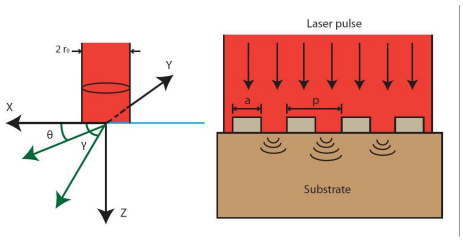

Figure 2.1: Laser radiated onto the grating structure on a substrate. The substrate is modeled as a semi-infinite homogeneous medium with z=0 coinciding with the surface of the substrate.

mal gradients. In this section, we first discuss the generation of surface waves from the theory of thermoelasticity. We will derive the expression for surface displacement of the substrate and develop the spectral form of the surface acoustic wave in terms of the temperture field at the surface. We start with the non-stationary problem of thermoelasticity to consider the behavior of Rayleigh waves on a surface. The fundamental equations of thermoelasticity for isotropic materials in the vector form are:

$$\mu\nabla^2 u + (\lambda+\mu)\nabla(\nabla.u) = \rho\ddot{u} + \gamma\,\nabla\theta \tag{2.1}$$

$$\nabla^2\theta - \frac{1}{\chi}\dot{\theta} - \eta\nabla.\dot{u} = \frac{-Q}{\chi} \tag{2.2}$$

where **u** represents the displacement field, θ is the temperature increment, Q is the volumetric heat source, and λ and μ are the Lame' constants of the medium. The thermal diffusivity is given by χ, while , $\gamma = (3\lambda+2\mu)\beta$, β being the volume expansion coefficient of the medium. It is convenient to write the wave equation, Eqn.(2.1), in terms of a scalar potential ϕ and a vector potential ψ such that $u = grad\,\phi + curl\,\psi$. Thus, Eqn.(2.1) is written as

$$\frac{1}{c_l^2}\frac{\partial^2\phi}{\partial t^2} - \nabla^2\phi = \left(1 - \frac{4c_t^2}{3c_l^2}\right)\beta\,\theta \tag{2.3}$$

$$\frac{1}{c_t^2}\frac{\partial^2\psi}{\partial t^2} - \nabla^2\psi = 0 \tag{2.4}$$

The longitudinal and transverse velocities are given by $c_l = \sqrt{(\lambda+2\mu)/\rho}$ and $c_t = \sqrt{\mu/\rho}$ respectively.

Consider a homogenous, isotropic elastic space with the x-y plane representing the surface of the substrate while the z-axis is directed into the medium. We apply the following boundary conditions at z=0 to solve Eqns.(2.2)-(2.4): (a) A traction free surface which implies $\sigma_{zx} = \sigma_{zy} = \sigma_{zz} = 0$; (b) An adiabatic temperature condition $(\partial T/\partial z)|_{z=0} = 0$ with the initial temperature $T(t = 0) = 0$. It should be noted that the adiabatic boundary conduction is only valid for samples of thicknesses $L >> (\chi\, t_{max})^{1/2}$, t_{max} being the thermal transit time through the bulk of the sample which is true in this case.

For writing the boundary condition for $\sigma_{zx} = \sigma_{zy} = \sigma_{zz} = 0$, we use Duhamel Neumann relation $\sigma_{ij} = 2\,\mu\, e_{ij} + (\,\lambda\, e_{kk} - \gamma\,\theta)\,\delta_{ij}$, where strains $e_{ij} = (u_{i,j} + u_{j,i})/2$. Thus, we can write the expressions for stress free boundary conditions in terms of potentials. Hence writing the boundary conditions (at z=0)

$$At\ z = 0, \quad \frac{\partial}{\partial z}(\nabla_\perp \phi) = (\frac{1}{2c_t^2}\frac{\partial^2}{\partial t^2} - \nabla_\perp)\zeta \tag{2.5}$$

$$At\ z = 0, \quad \frac{\partial \zeta}{\partial z} = -(\frac{1}{2c_t^2}\frac{\partial^2}{\partial t^2} - \nabla_\perp)\phi \tag{2.6}$$

Here, $\nabla_\perp = \frac{\partial^2}{\partial x^2} + \frac{\partial^2}{\partial y^2}$ and $\zeta = \frac{\partial \psi_y}{\partial x} - \frac{\partial \psi_x}{\partial y}$.

The scalar equations of ϕ in Eqn.(2.3) and for ζ in Eqn.(2.4), coupled with boundary conditions, Eqn.(2.5) and Eqn.(2.6) describe the excited bulk and Rayleigh wave. Rayleigh waves are a result of interaction of longitudinal and transverse waves at the surface. The efficiency of the surface waves is dominated by the transverse inhomogenities in potentials at the surface.

Since we are interested in the frequency characteristic of SAW, we seek the spectral form of **u**. We define operator which taken Fourier transform in time and in transverse coordinates r=$\{x, y\}$ and Laplace transform in z.

$$\begin{aligned}\tilde{A}(\omega, k_x, k_y, s) = \int_0^z dz \int_{-\infty}^{\infty} exp(i\,\omega\, t) exp(-i\, k_x\, x) exp(-i\, k_y\, y) \\ \times exp(-s\, z) A(x, y, z, t) \mathrm{d}t \mathrm{d}x \mathrm{d}y\end{aligned} \tag{2.7}$$

The spectral form of surface displacement at z=0 from the relation u=grad

$\phi + \text{curl } \psi$ is $u_z(\omega, k) = \frac{d\tilde{\phi}}{dz}|_{z=0} + \tilde{\zeta}|_{z=0}$. Solving the system of Eqns.(2.3)-(2.6), we obtain the spectral form as [21]

$$\tilde{u}(\omega, k_\perp)|_{z=0} = -\beta\, N\, (1 - \frac{4c_t^2}{3c_l^2})\hat{\theta}(\omega, k_\perp, (k_\perp^2 - k_l^2)^{1/2}) \tag{2.8}$$

where $\hat{\theta}$ is the spectral transform of temperature field, N is constant that depends on elastic properties of the substrate.

Thus, the spectral form of surface displacement has linear dependance on the temperature field. Moreover, if we examine the displacement of surface z=0, the frequency of surface acoustic waves is determined by the frequency components of temperature field. In the next section, the temperature field at the surface of the substrate is derived using the proposed model for heat generation.

2.2 Opto-Acoustic Generation

In this section, we model the periodic temperature profile along the surface of the substrate which in turn leads to excitation of SAW. Using the solutions derived in previous section, we attempt to understand the frequency characteristics of surface acoustic waves and identify the parameters that are critical in affecting their frequency.

We consider a grating of period 'p' on a absorbing substrate as shown in Fig.2.1. The width of each line in the grating is 'w' while the thickness is 'h'. α_g and α_s are absorption coefficients of grating and substrates respectively. The reflectivities R_g and R_s are defined in same manner. The laser energy is given by Q_0. The optical spot radius is r_o. Spaces r^1 indicates the surface regions of substrate not covered by grating while r^2 indicates the region of substrate under the grating.

2.2.1 Heat Absorption Model

In this sub section, we will discuss the heat generation Q occurring in the substrate due to optical absorption of the laser. We consider a laser pulse

of Q_0=1 nJ incident on the grating normally. The critical parameters for analyzing the heat generation are (i) the depth of heat absorption, (ii) how it varies laterally and (iii) time till heat generation happens.

The depth of heat absorption depends on absorption coefficients of grating and substrate and is given by Beer-Lambert relation. We will define the depth dependence of Q (r,t,z) by a function F_z(z). It also depends on the phonon-electron coupling coefficient G which is not considered in this work. The lateral variation of heat generation F_r(r) depends on the profile of grating. The radial variation of heat generation imitates the grating structure, meaning the period of variation matches the period of grating. Finally the time period of heat generation depends on the duration of laser pulse. Equations (2.9) and (2.10) give the relations of the functions defined above for a Q-switched laser. The subscripts s and g represent substrate and grating respectively.

$$Q(r,t,z) = F_r(r)F_t(t)F_z(z) \tag{2.9}$$

where we define

$$\begin{aligned}
F_r(r) &= \begin{cases} \frac{(1-R_s)Q_0}{\pi\, r_0^2} exp(-\frac{r^2}{r_0^2}) & for\, r \in r^1 \\ \frac{(1-R_s)(1-R_g)exp(-\alpha_g\, h_g)Q_0}{\pi r_0^2} exp(-\frac{r^2}{r_0^2}) & for\, r \in r^2 \end{cases} \\
F_t(t) &= (t/t_0^2)exp(-t/t_0) \\
F_z(z) &= \alpha_s exp(-\alpha_s z)
\end{aligned} \tag{2.10}$$

Now, we will derive the temperature field in the substrate using the heat diffusion equation in Eqn.(2.11) with the heat generation Q given in Eqn.(2.10). This field varies with r=$\{x, y\}$,z and t. As we sought the solution in spectral form, the respective coordinates are wavevector $k_\perp$=$\{k_x, k_y\}$, laplace variable s and ω. We solve the heat diffusion equation by applying the initial boundary condition T(t=0)=0, the adiabatic boundary condition dT/dz=0 at the surface and the condition that T$\rightarrow$ 0 as z$\rightarrow \infty$. The spectral form of the temperature field is thus derived as

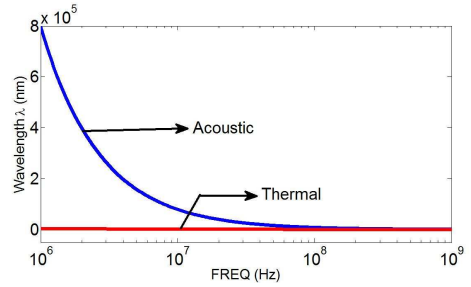

(a)

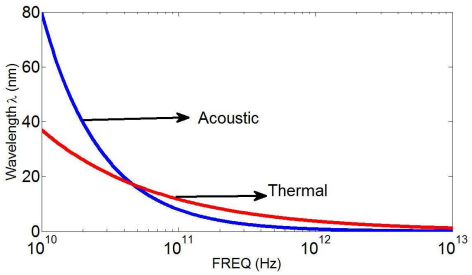

(b)

Figure 2.2: (a) **MHz-GHz range:** The thermal wavelength is insignificant in comparison to that of acoustic wavelength at lower frequencies of SAW (b) **Beyond GHz:** The thermal and acoustic wavelengths are comparable for frequencies above 10 GHz.

$$\hat{\theta}(\omega, k_\perp) = \frac{\tilde{F}_r(k_\perp)\tilde{F}_t(\omega)\tilde{H}_z(k_\perp, k_\theta)}{\rho\, c\, \chi} \tag{2.11}$$

where

$$\tilde{H}_z = \frac{\sqrt{k_\perp^2 - i\,k_\theta^2}\tilde{F}_z\left(\sqrt{k_\perp^2 - k_l^2}\right) - \sqrt{k_\perp^2 - k_l^2}\tilde{F}_z\left(\sqrt{k_\perp^2 - i\,k_\theta^2}\right)}{\sqrt{k_\perp^2 - i\,k_\theta^2}\,(i\,k_\theta^2 - k_l^2)} \tag{2.12}$$

where $k_\perp$ is the acoustic wavevector while $k_\theta^2 = \omega/\chi$, χ being the thermal diffusivity and $k_l = \omega/c_l$. Here $\tilde{F}_r(k_\perp)$, $\tilde{F}_t(\omega)$, and $\tilde{F}_z(s)$ are spectral transforms of $F_r(r)$, $F_t(t)$, and $F_z(z)$ respectively.

This periodic temperature field shown in Eqn.(2.11) leads to generation of surface waves . From Eqn.(2.8) we see that the period of SAW exactly matches with that of temperature field. Hence it is important to analyze the factors that affect the temperature field from its spectral form. In Eqn.(2.11), we analyze each factor separately in order to understand the effects of each parameter on the frequency of the SAW.

The assumptions that thermal properties of medium do not affect the SAW frequency simplifies Eqn.(2.11) to Eqn.(2.13) by imposing the condition that the magnitude of Rayleigh wave vector $k_\perp = \omega \,/\, c_R$ is very small than that of thermal wave vector, $k_\theta >> k_\perp$.

$$\hat{\theta}(\omega, k_\perp, s) = -\frac{i}{\rho\, c\, \omega}\, F_r(k_\perp)\, F_t(\omega)\, F_z(s) \tag{2.13}$$

However, this assumption is invalid in the GHz range. Figure 2.2 shows that magnitudes of thermal and acoustic wave vectors are comparable in high GHz frequency range. Hence, we use the complete form of Eqn.(2.11) in predicting the waveform of the surface wave.

2.3 Analysis of SAW field

Firstly, we discuss the effect of rise time of the pulse on the spectral components of temperature field from Eqn.(2.11). From the factor $\tilde{F}_t(\omega)$, we can say that shorter the rise time of the pulse t_0, higher is the frequency components contributed by the factor $\tilde{F}_t(\omega)$ in Eqn.(2.11), as seen in Fig.2.3. However a conclusion cannot be made that higher frequency SAW can be obtained as we keep on decreasing the length of pulse. This is due to the fact that the frequency of SAW depends on other factors which multiply with $\tilde{F}_t(\omega)$. Thus we can conclude that for generating SAW of near THz frequency, a minimum condition is that laser pulse should have a rise time less than 100fs.

Next we discuss the frequency components contributed by the depth function $\tilde{F}_z$(s) which affects the temperature field as shown in Eqn.(2.11). The observation using this model is that the higher absorption coefficient, a contribute higher frequency components for the surface acoustic wave, as seen in Fig.2.3(b). The other parameters higher Rayleigh velocity of substrate, V_R and lower thermal conductivity k_{cond} give rise to higher amplitude of SAW mode at a particular frequency. A surface acoustic wave has energy decaying into the bulk in z-direction as E=E_0exp(-z/λ) where λ is the wavelength of the wave. Thus the penetration depth of a surface wave is $\lambda/2\pi$. For strong focusing, a should satisfy $\frac{1}{a} < \frac{\lambda}{2\pi}$. Effect of thermal conductivity of substrate has significant impact on frequency of SAW only beyond 0.3 THz.

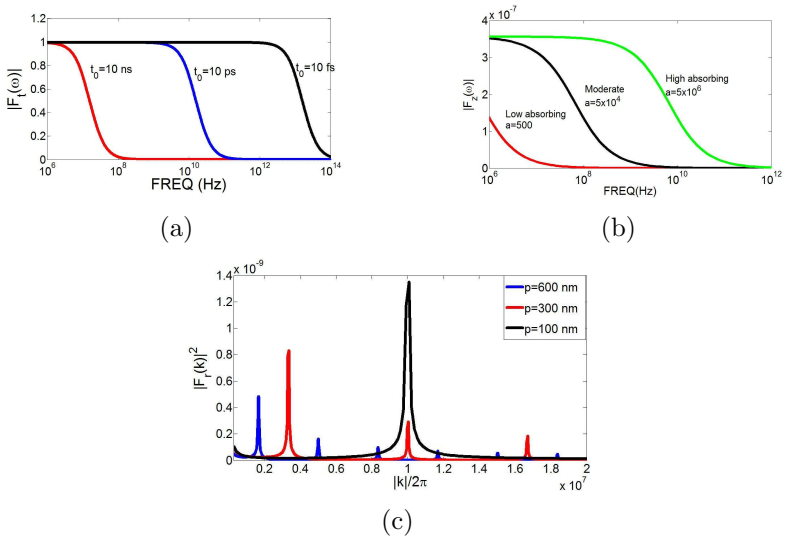

Figure 2.3: (a) Frequency Dependence of $\tilde{F}_t(\omega)$ with variation in rise time of pulse. The plot shows that the frequency contribution by the factor $\tilde{F}_t$ increases as the length of the pulse shortens. (b) Effect on $F_z(\omega)$ with increasing absorption coefficients at k=10 W/m/K. (c) Spectral Dependence of the F_r(r) shows that the decrease in period of grating leads to higher frequency components of SAW.

Finally the foremost factor, the period of grating will affect the function F_r(r) and thus its corresponding transform $\tilde{F}_r$(k) where k is the radial wavevector. With decrease in the period of the grating, p, the frequency component of $\tilde{F}_r$(k) will increase as shown in Fig.2.3(c). The peak in frequency of $\tilde{F}_r$(k) occurs at $|k| = 2\pi/p$ where p is the period of the grating. The amplitude of the surface wave will also increase with decrease in period due to the fact that the number of grating line exposed to the laser pulse will increase. Another factor that affects $\tilde{F}_r$(k) is the laser spot radius, r_0. A smaller laser spot radius r_0 is desired for high amplitude SAW because of increased intensity incident on the grating. However, this increased intensity may cause ablation of the grating and surface. Hence the laser spot radius is fixed at 5 μm so that no ablation occurs and the SAW generation is thermoelastic. The power of SAW is also affected by the duty cycle of the grating ($\eta = \frac{w}{p}$) since $F_r(r)$ in Eqn.(2.10) depends on the width of the grating. For maximum efficiency, duty cycle η should be 0.5.

We discussed the critical parameters involved in $\tilde{F}_r$(k), $\tilde{F}_t(\omega)$ and $\tilde{F}_z$(s)

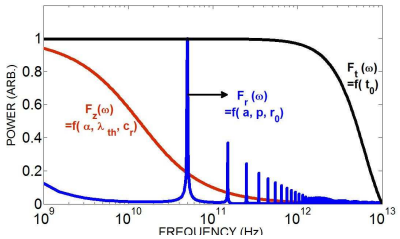

Figure 2.4: This graph shows the summary of the frequency dependance of the the three functions and the parameters influencing them. The resultant SAW is the product of the three curves here. In this figure, t_0=100fs rise time laser incident on high absorbing substrate ($\alpha = 5 \times 10^6 m^{-1}$) with spatial period p=100 nm.

that will affect the frequency components of temperature field as well as the SAW. But from Eqn.(2.11) for spectral form of temperature field, we have product of these factors implying that at the frequency of the surface acoustic wave ω_R, we should have all the three factors significant. For grating period greater than 100nm, from the frequency response functions, we can see that $\tilde{F}_r$(k) is the limiting factor. Hence, in this case, the product of the three factors is dominated by $\tilde{F}_r$(k) and thus the frequency of surface acoustic wave is strictly restricted by the period of the grating. If the rise of time of pulse t_0 and absorption coefficient α satisfy the minimum conditions as mentioned above, these factors will no longer affect the frequency of surface acoustic wave. Thus in this case, the frequency of surface acoustic wave is $f_{SAW} = |k|\, V_R/2\pi = V_R/p$ where V_R is the Rayleigh velocity of the substrate. But at high frequencies, all the material parameters have an effect on the amplitude of the surface acoustic wave.

Following the discussion on the critical parameters that affect the frequency of surface acoustic wave, we predict that surface acoustic waves of upto 275 GHz can be generated if a femtosecond laser of rise time $<$ 100 fs is used on a Aluminum($\alpha_g = 5 \times 10^7, R_g = 0.3$) on nano-crystalline CVD diamond film with grating period of about 40 nm. CVD diamond is used because it is known to have the highest Rayleigh velocity of $\sim 11,000$ m/s. But it also exhibhits very high thermal conductivity. However, it is seen that the thermal conductivity will not have as significant impact on frequency of SAW as the Rayleigh velocity.

2.4 Damping of SAW waves

The challenging aspect of generation of surface acoustic waves beyond 100 GHz regime is acoustic attenution of elastic energy at the surface. We talk about three different attenuation mechanism in the scheme considered. The first mechanism thermoelastic damping occurs due to diffusion of thermal field with time and its rate depends on interface resistance of grating and substrate and the thermal conductivity of substrate. A simple model predicts that the damping of the SAW through this mechanism is proportional to the square of frequency of the wave and the density of the grating. Akheiser effect is also a significant effect in disspiation of surface waves, especially in THz range as the coherently-excited acoustic wave disturbs the phonon equilibrium resulting in energy dissipation [18].

The another mechanism that attenuates the surface acoustic waves is their coupling to bulk waves and eventual dissipation into bulk. The model in this paper does not take the effect of grating structures on the propagation of the waves. However, the presence of grating structures on the substrate can effect the SAW propogation significantly. The SAW mode was not observed in case of gold nanostructures on fused-quartz [14]. They argued that strong coupling to bulk longitudinal modes greatly inhibited SAW generation efficiency. The attenuation coefficient in this mechanism is found to have fourth power dependence on the frequency of the wave and density of the grating [18, 15]. Thus in high frequency regime, this effect completely dominates the dissipative attenuation [22]. In the subsequent chapters, we study experimentally and theoretically the effect of grating structures on the propagating surface waves and discuss in detail the attenuation mechanisms of the wave.

2.5 Conclusion

When a ultrashort pulse laser is incident on a nanostructure grating on a substrate, the differential absorption of pulse in grating and substrate sets up a periodic thermal field at the surface of the substrate. This periodic thermal stress launches a surface acoustic wave with the same frequency as

that of the thermal field. Upon the analysis of the spectrum of SAW on the surface of substrate, the critical parameters that affect the frequency of SAW have been determined. In order to achieve surface waves in $100-300$ GHz range, femtosecond laser pulses incident on the grating structure on the substrate should have a period less than 50 nm. In addition to this, it is desirable to have a substrate with high Rayleigh velocity, good optical absorption and low thermal conductivity.

CHAPTER 3

EXPERIMENTAL RESULTS

3.1 Introduction

In this chapter, an experimental study of the dynamics of surface acoustic waves in the periodic composite (grating on substrate) is presented. Specifically, the frequency and the life time of the surface oscillations is studied in Al nanostructures on Si substrate using time resolved reflectivity measurements. As discussed in the previous chapter, the wavelength of the photoexcited SAW matches the period of the Al grating (p) and the frequency of the SAW (f) is given by $f = V_R/p$ where V_R, the Rayleigh velocity in silicon is 4910 m/s. Since this work is pertained to hypersonic frequency regime (ν >10 GHz), there is a need to fabricate Al lines with periods less than 400 nm.

As discussed in the previous chapter, one of the major limitations in scaling up the frequency of SAW is the mass loading from the periodic metal overlay which causes a damping proportional to the ratio of square of metal density and fourth power of the period of the grating. Since we need lower periods of grating for excitations of hypersonic frequencies, the main factor that we can tailor to reduce the mass loading is the metal density. Hence low density metals like Al are used a stressors. In generality, for the low density metals, the amount of perturbation that the metallic overlay causes to the propagating waves is considered negligable and is treated by thin film perturbation theory. Theoretical predictions on the nature of mass loading using perturbative approach are well estabhished in the literature.

However, at frequencies > 10 GHz, the penetration depth of the surface acoustic wave ($\sim$ 300 nm) is very less into the Si, the wave is increasingly

localized in the metallic overlay. As a result of this excessive coupling of SAW with the metal overlay, the perturbation of the wave by the metal is too significant to modeled by a perturbative approach. To this date, a reliable study on the geometry of metal overlay on the frequencies and the life times of surface oscilations is not available. In this experimental study, we attempt to address the effect of coverage ratio (or duty cycle) of the Al grating on the dynamics of the SAW propagating in silicon.

3.2 Fabrication

Since standard photolithography cannot be used to pattern Al lines of feature size less than 500 nm, we use e-beam lithography to pattern the photoresist on the Si surface. First, poly methyl methacrylate (PMMA) is spinned onto silicon substrate with a thickness of 400 nm. The polymer is patterned to define the grating structures using e-beam lithography (JEOL JBX-6000FS Electron Beam Lithography System). The grating structures for this experiments were targeted to have a period of 300 nm and 400 nm. The width of the Al lines in the experiments were varied form 80 nm to 320 nm. This step is followed by deposition of 50 nm aluminium onto this patterned surface using CHA e-beam evaporator. Finally, we perform liftoff to remove the PMMA. Figure 3.1(a) shows the outline of the fabrication procedure. The high resolution SEM images of 300 nm and 400 nm gratings are shown in Figure 3.1(b).

3.3 Picosecond Ultrasonics

As discussed in Chap 2, the generation and the detection of the surface oscillations is acheived by picosecond ultrasonics. In this technique, a short laser pulse (with rise time in orders of femtoseconds) is irradiated onto Al-Si structure. This laser pulse, called “pump” beam heats up the Al line by about 100 K while the rise in temperature of Si is negligable if the laser wavelength is in infrared regime. The “pump” beam is followed by a “probe” beam, which has less power compared to the “pump” with a time delay (t)

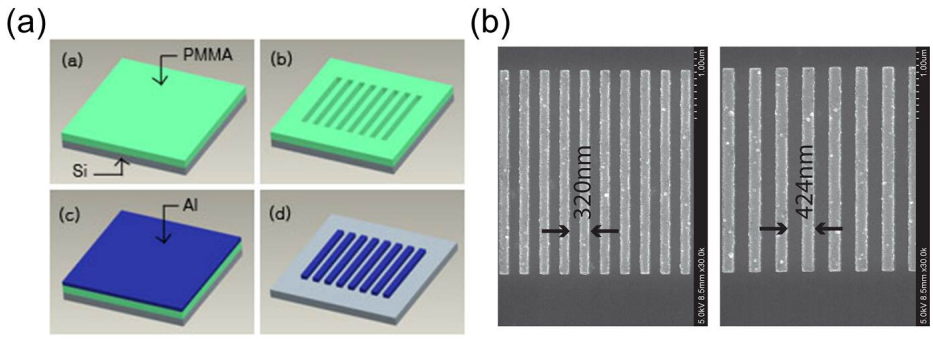

Figure 3.1: (a) The Al lines on Si are patterned by e-beam lithography followed by Al deposition and lift off steps. (b) The SEM images of the samples showing the period of gratings.

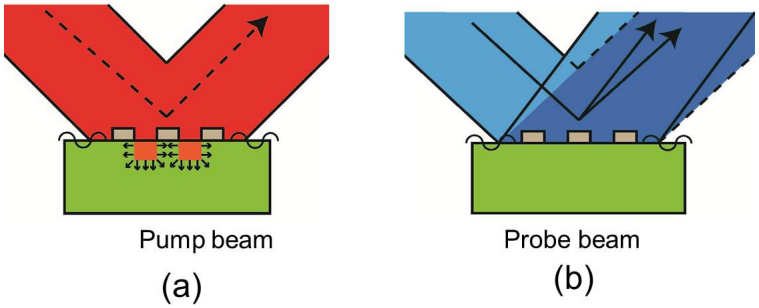

Figure 3.2: (a) The pump beam heats up the Al lines by over 100 K. The heat is eventually dissipated through Al-Si interface (b) The probe beam monitors the strain induced reflectance change of surface in time.

between the two pulses. The probe beam reflects off the Al/Si surface and is picked up by a photodiode. Due to thermal strain generated by temperature rise of Al, the consequent generation of SAW strain pulse will induce change in the optical properties (complex refractive index n+ik) depending on the magnitude of the strain. As a result of this change in optical properties, the probe reflectivity varies in time thus yielding the information about the surface oscillations. The "pump" and the "probe" are incident on the same spot ($\sim 7\mu m$ diameter spot) on the structure as shown in Fig 3.2.

The pump and probe beams are derived from a synchronously mode locked Ti-Sapphire femtosecond laser (Tsunami laser, FSMRL Laser facility) with a rise time of laser pulse of about 100 fs. The laser pulse train has a repetition

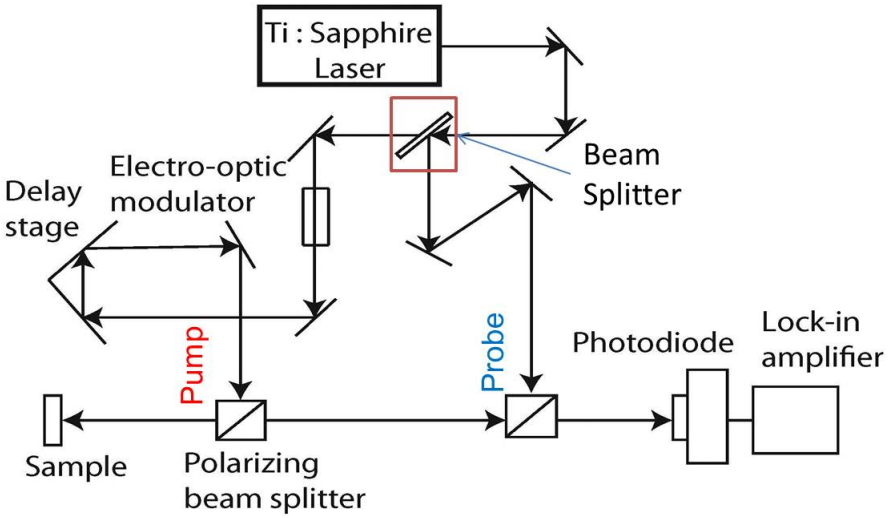

Figure 3.3: The optical circuit for TDTR experiment is shown. Both pump and probe focused onto the sample have a time delay controlled by mechanical stage.

rate of 80 MHz and wavelength 785 nm. The pump light is amplitude modulated at 9.8 MHz to facilitate lock-in detection and the delay between the arrival of the pump pulse and the probe pulse is controlled by a mechanical delay stage. The delay time between pump and probe is increased linearly upto 1600 ps followed by exponential stepping upto 3600 ps. The acoustic oscillations in this experiment typically last for 1000 ps and thus fine stepping of 0.5 ps is maintained till this delay time is reached. The optical circuit of the whole setup is shown in Fig 3.3.

3.4 Acoustic Signals from TDTR data

A typical TDTR signal is shown in Fig 3.4(a). This signal is the manifestation of the strain induced change in optical properties of the grating and the substrate. As seen in Fig 3.4(a) the signal composes of a slowly varying thermal decay which represents the heat diffusion from Al to Si along their interface and the heat diffusion into the bulk of Si. The thermal background is carefully removed by fitting apporporiate exponentials corresponding to the diffusion rates. The acoustic signal obtained by this removal is shown in

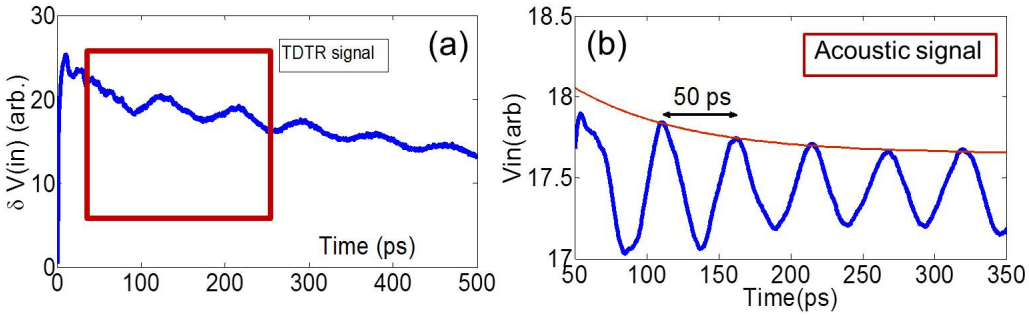

Figure 3.4: (a) The typical TDTR signals showing acoustic oscillations and decay in temperature. (b) The acoustic signal extracted from TDTR signal by removing thermal background.

3.4(b).

The oscillations in the TDTR signal represent the acoustic data. To understand this acoustic data, we consider two regions (a) delay time t <80 ps (b) delay time t >80 ps. In region (a), the oscillations in Fig 3.4(b) correspond to the longitudinal oscillations in Al. As the optical absorption of the laser pulse in Al begins at t=0, there is sharp rise in the strain in the Al film. This is a result of heating up of electron gas which diffuses into metal undergoing collisions with lattice thereby reaching to electron-phonon equilibrium within t=5 ps. Subsequently, the thermal expansion of Al sets up a longitudinal acoustic pulse travelling into the Al towards Al-Si interface. These oscillations travel back and forth with a time period $T_{Al} = 2h_{Al}/V_{l,Al}$ where h_{Al} is the height of Al film, $V_{l,Al}$ is the longitudinal velocity of sound in Al (6420 m/s). We observe this time period corresponds to T = 12.2 ps (59.6 GHz).

In region (b), we observe a collection of frequencies with a dominant frequency corresponding to the frequency of SAW as seen in Fig 3.5. Specifically, for gratings with period $p = 400$ nm and $p = 300$ nm, we observe acoustic oscillations in time-resolved reflectivity signal with time periods $\Delta T = 81.6$ ps and $\Delta T = 59.6$ ps respectively. We attribute these oscillations to surface acoustic wave propagating in Si since the frequency of oscillations have inverse dependence on the period of the grating. Further, the time period of oscillations $\Delta T = p/V_r$ of the unperturbed waves show a close match for

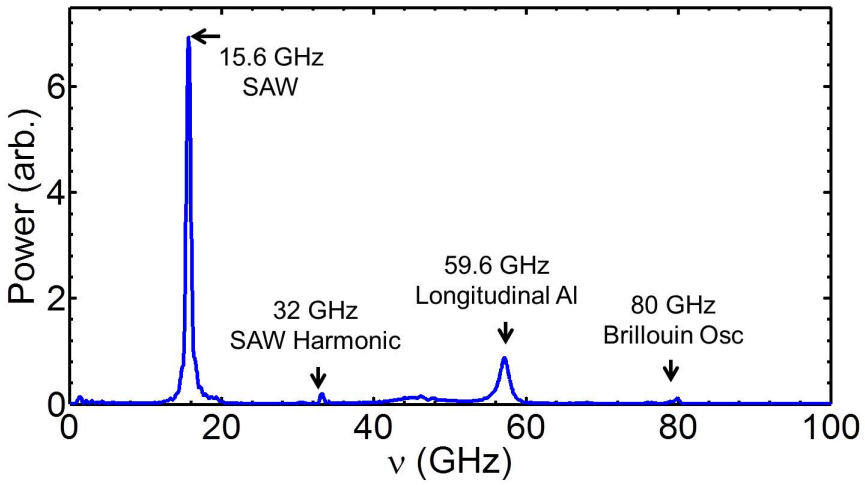

Figure 3.5: The power spectrum of TDTR signal for 300 nm grating without thermal background.

V_r = 4920 m/s (Rayleigh velocity in Si) with 82 ps (ν = 12.2 GHz) and 61 ps (ν = 16.3 GHz) for the p=400 nm and p=300 nm gratings respectively. This confirms the excitation of SAW at the center of Brilloiun zone of the structure ($k_x = 2\pi/p$).

In addition to the SAW frequency, we observe higher frequencies that correspond to the higher harmonics of SAW with a wavevector $k_x = 2m\pi/p$ where m=2,3,... There is a frequency component corresponding to 80 GHz Brilloiun oscillations. This is detected as a result of reflection of probe from the longitudinal strain pulse traveling in Si. The time period of this oscillation for a normally incident probe is given by $T_L = \lambda/2nV_{L,Si}$ where λ is the probe wavelength (785 nm), n is the real refractive index of Si and $V_{L,Si}$ is the longitudinal velocity of sound in Si. The Fourier transforms of acoustic signals in 300 nm and 400 nm gratings is shown in Fig 3.6.

3.5 Duty cycle effect on SAW characteristics

In order to study the dynamics of SAW propagation under a periodic overlay with different coverages, we consider samples of Al-on-Si substrate with pe-

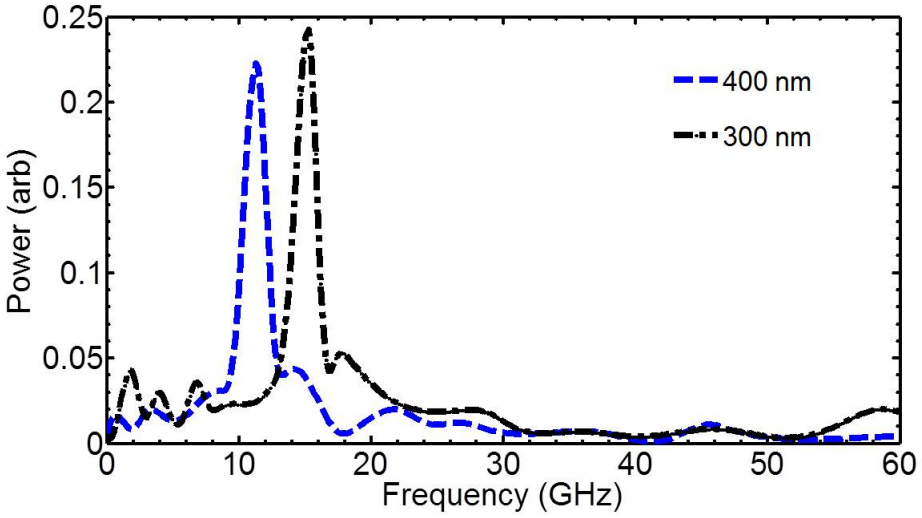

Figure 3.6: The power spectrum of acoustic signals for 300 nm and 400 nm grating.

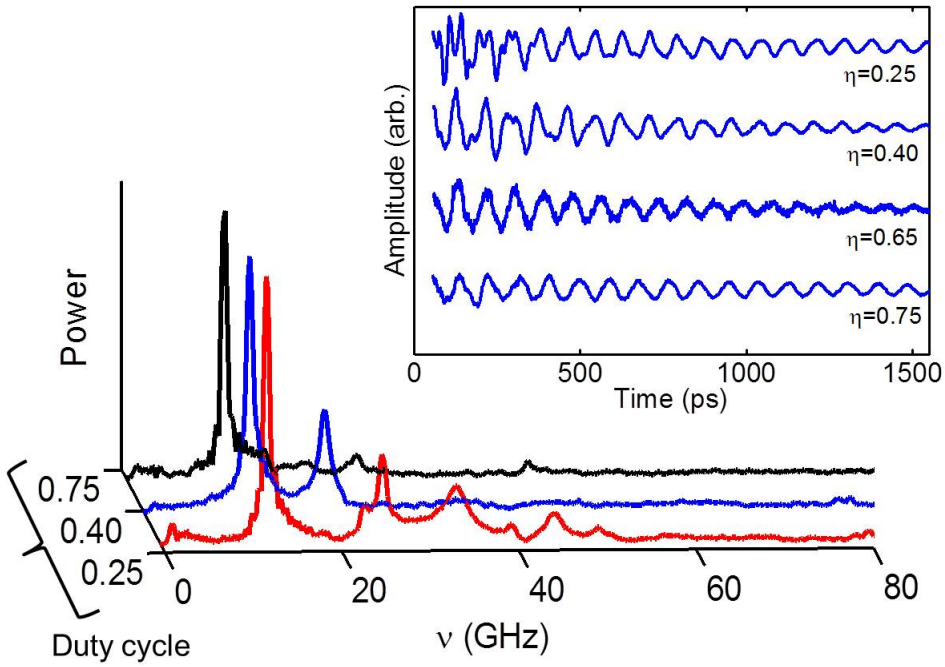

plot.pdf

Figure 3.7: The acoustic signals and their corresponding transforms for 400 nm gratings at different duty cycles is shown.

Sample #	Period (nm)	Duty cycle	Frequency (GHz)	Damping time (ps)
1	400	0.31	12.01	1320±90
2	400	0.48	12.09	688±80
3	400	0.76	11.15	1580±60
4	300	0.32	15.69	645±60
5	300	0.54	15.87	282±30
6	300	0.71	15.15	662±60
7*	400	0.55	11.94	552±80
8*	400	0.57	11.85	594±80
9*	400	0.61	11.67	627±80
10*	300	0.60	15.8	296±40

Figure 3.8: The experimental sample description with the peak SAW frequency and damping time is tabulated. (The samples with * have higher scale of roughness on Al lines.

riods 300 nm and 400 nm and duty cycle (defined as ratio of width of Al and period of Al grating) varying from 0.2 to 0.8. The sample information about the period and the duty cycle is given in Fig 3.8. The thermal background from each of the TDTR signals obtained from the samples is removed by fitting different exponential functions in each case. The resultant acoustic signals are zeropadded and then transformed to Fourier space to obtain the peak frequency of SAW with an accuracy in two decimal places. The Fourier transforms of acoustic signals for the 400 nm samples at three different duty cycles is shown in Fig 3.7. The experimentally determined frequencies are shown in Fig 3.8

3.5.1 Frequency dispersion

The coupling of the surface acoustic wave with Al grating renders frequency shift ($\Delta\nu$) of the wave from the unperturbed state (without Al grating). This frequency shift is primarly because of the mass loading from the grating and the stress loading. The latter phenomenon is caused by the impingment of

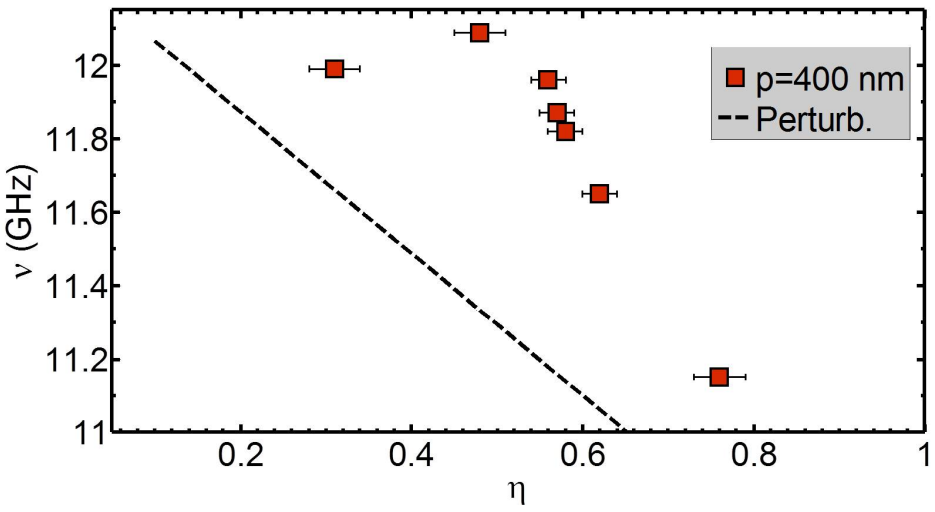

Figure 3.9: The frequency dispersion with the duty cycle is grating for 400 nm gratings. Also shown is the prediction by perturbation theory.

SAW with a periodic Al line causing shear stresses at the Al-Si interface at that line which in turn causes the wave to reflect. The ratio of amplitude of the reflected and the incident wave is called the reflection coefficient. Hence the frequency shift is caused by mass loading and the reflection coefficient.

Due to significant localization of the SAW near the surface at high frequencies ($\sim$ 300 nm), the observed frequency of SAW mode vary significantly with interaction of wave with Al overlay. Fig 3.9(a) shows a plot of SAW frequency shift from the unperturbed value with the duty cycle of the 300 nm and 400 nm gratings. The duty cycle and the period of the gratings are determined from high resolution SEM images while the height of the lines is determined to be $h = 54$ nm by observing acoustic peaks corresponding to longitudinal oscillations in Al. From Fig 3.9(a), we observe that the frequency shift of the SAW mode due to mass loading from the periodic overlay is not linearly dependant on the duty cycle as predicted by perturbation theory for Si-Al system. According to modified thin film perturbation theory [23], the shift in the frequency of SAW $(\nu(p) - \nu(0))/\nu(0) = F_v(h/p)\eta$ where $\nu(p)$ is the perturbed frequency while $\nu(0)$ is the ratio of Rayleigh velocity in Si to the period of the grating. F_v is the first order mechanical scattering coefficient and is -1.26 for Si-Al system[16]. The experimentally determined frequen-

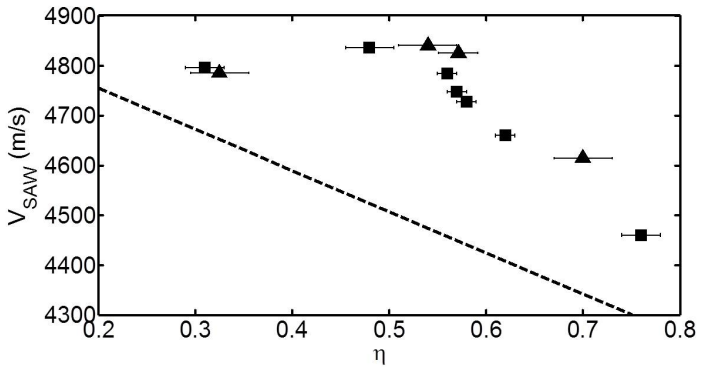

Figure 3.10: The SAW velocity dispersion with the duty cycle is grating for 400 nm and 300 nm gratings. The unperturbed velocity of SAW in Si is 4910 m/s.

cies deviate from the perturbation theory significantly for 400 nm grating as shown in Fig 3.9. Hence we conclude that the effect of Al overlay on propagating SAW of frequencies greater than 10 GHz is too significant and the coupling of Al and Si modes is very strong. Thus the full eigen calculation of the frequencies of the composite structure is required to explain this effect which is the purpose of Chap 4. The corresponding SAW velocity shift for 300 nm and 400 nm grating with the prediction from pertubation theory is shown in Fig 3.10.

3.5.2 Experimental SAW attenuation

Further, the damping time of the acoustic wave can also be obtained from the data. The attenuation of a surface acoustic wave is a very important parameter in design of SAW resonators. The calculation of attenuation (inverse of damping time) can be carried in two ways. The attenuation of a SAW mode is the FWHM (full width half maximum) of the frequency spectrum around the peak SAW frequency. We carry out an other more accurate method to extract the damping. We fit the acoustic data with synthetic wave form $\Delta R = Asin(2\pi\nu t)exp(-t/\gamma) + \sum_{i=2}^{n} a_i sin(2\pi\nu_i t)exp(-t/\gamma_i)$. Here the first term corresponds to SAW with A being its amplitude, ν is the SAW frequency and γ is the damping time of the wave. The second term is a summation of other frequencies in spectrum (higher harmonics of SAW) which

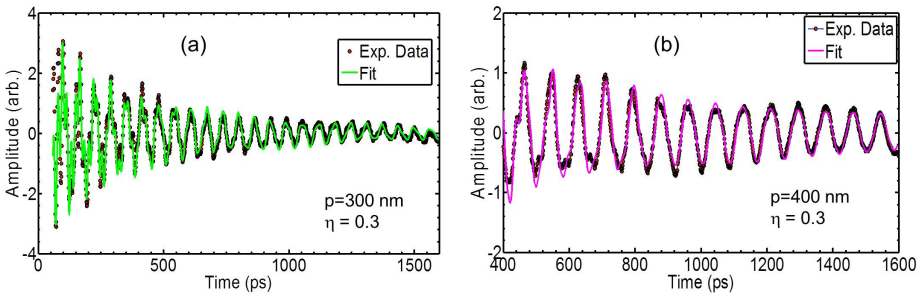

Figure 3.11: The acoustic signal is fitted by a synthetic waveform to obtain attenuation of the wave.

have very low amplitude and damp very quickly. The fits obtained by using this synthetic waveforms is shown in Fig 3.11

Having extracted the damping times by fitting the synthetic waveforms, we plot the damping time (inverse of attenuation) with the duty cycle for 300 nm and 400 nm gratings as shown in Fig 3.12. We observe that attenuation is largest around $\eta = 0.5$ suggesting that for both periods, $\eta = 0.4 - 0.6$ should be avoided for design of high frequency phononics. There is about a 40% increase in the lifetime of the oscillations from $\eta = 0.5$ to $\eta = 0.76$ in 400 nm grating. Further there is 60% reduction in the lifetime of oscillations from 400 nm to 300 nm gratings showing the effect of grating becomes more significant at higher frequencies thus limiting the capabilities of SAW generation by this technique.

In summary, we demonstrated the picosecond ultrasonics technique for analyzing acoustics in hypersonic regime by probing for strain induced reflectivity change of the structure. The acoustic data was obtained by removing the thermal background from the time resolved reflectivity signals. We proved that the observed oscillations in the signals correspond to surface acoustic wave and has inverse dependence with the period of the grating. We analyzed the surface acoustic wave dynamics in Al-on-Si structure with varying duty cycle of the Al grating. We observed that the frequency shift ($\Delta\nu$) with increasing duty cycle is non linear instead of linear downward shift predicted by perturbation theory and maximum deviation occurs at $\eta = 0.5$. This led to the conclusion that the effect of Al grating on the high frequency SAW

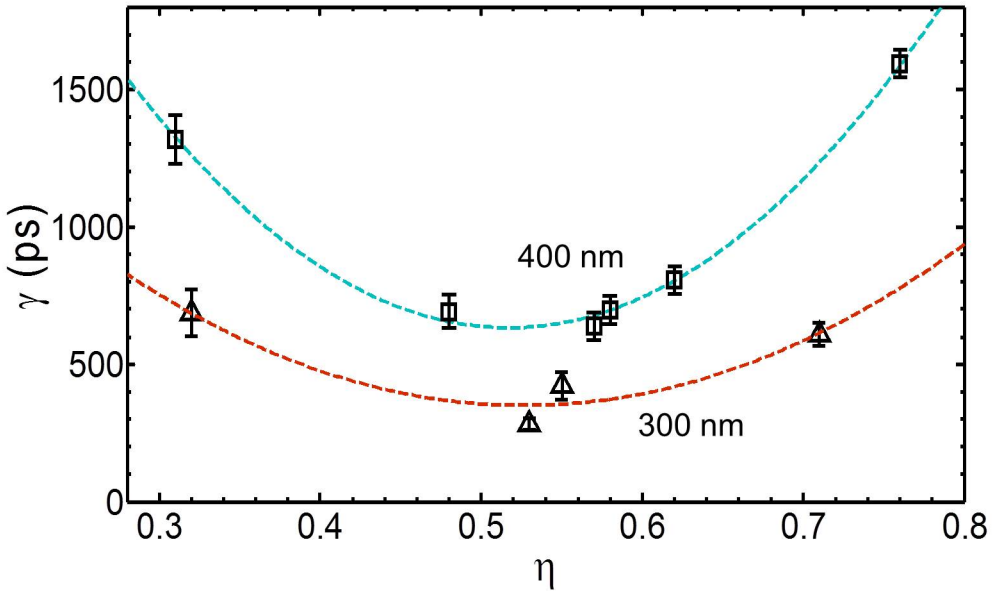

Figure 3.12: The lifetime of surface oscillations plotted against duty cycle for 400 nm and 300 nm gratings.

(ν >10 GHz) is too significant to be predicted by perturbation theory. Further the lifetime of the oscillations is extracted by fitting synthetic damped sine to the acoustic data. A similar conclusion was made regarding attenuation of SAW as the $\Delta\nu$ that the attenuation of the wave is maximum around duty cycle $\eta = 0.5$.

CHAPTER 4

MODAL ANALYSIS OF PHONONIC CRYSTALS

As discussed in the previous chapter, the experimentally found frequency shift ($\Delta\nu$)and attenuation of the surface acoustic wave photoexcited in Si-Al periodic composite does not follow the perturbation theory. This suggests that the effect of Al grating cannot be treated as a mere perturbation on the Si. This approximation is only valid when either the width of Al line is very small compared to the gap between them or when the gap between the lines is much less than the width. For the rest of the cases, the duty cycle effect on SAW due to mass loading of Al should take into account the elastic properties and the geometry of the grating. For this purpose, we conduct an eigenmode analysis on the Al-Si periodic composite and see how the simulation results compare to the experimental data.

4.1 Modeling of unit cell of periodic composite

In order to model the Si-Al periodic composite, we model a unit cell of the periodic composite shown in Fig 4.1 and apply periodic conditions on the vertical boundaries of this unit cell. The key focus of this simulation is to extract the normal modes of the composite. Normal modes are independant modes of motion a structure possesses and any form of external forcing field on the structure results in excitation of the normal modes only with different weights. The mode that has highest amplitude has highest phonon population and we call it "dominantly" excited mode. The idea is to analyze the frequency, modal displacements of the dominantly excited mode to understand the frequency shift and examine the energy distribution near surface to understand the attenuation of the dominantly excited mode. Since we are going to apply the periodic boundary conditions on the vertical walls, we will

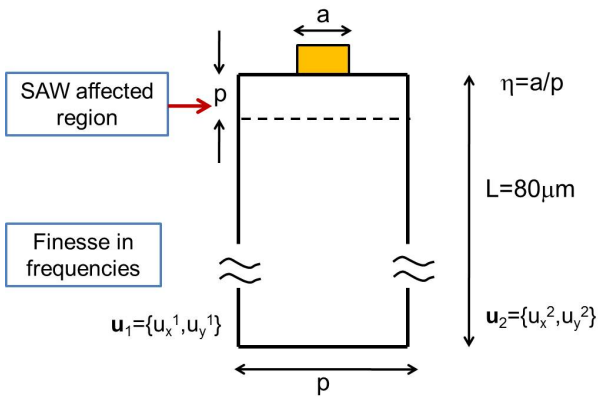

Figure 4.1: The unit cell of the periodic composite with a width equals wavelength of the modes to be analyzed.

be modeling for only the normal modes with wavevector $K = k_x + 2m\pi/p$, m=1,2,3... The surface mode we are interested in is the mode with m=1.

The number of discrete normal modes of a system depends on the size of the system. We seek second decimal point accuracy in the frequencies of the modes and thus we fix the length of the system to L =80 μm. The width of the grating line ('a') is varied to model of effect of duty cycle. The equation of motion to be solved for extracting modes of this structure and the corresponding eigenvalue problem are

$$\partial_j[c_{ijmn}(\mathbf{r})\partial_n u_m] = \rho(\mathbf{r})\ddot{u} \tag{4.1}$$

$$\partial_j[c_{ijmn}(\mathbf{r})\partial_n u_m] = -\rho(\mathbf{r})\omega^2 u \tag{4.2}$$

To this purpose, we adopt finite element formulation of this problem using ANSYS package. We use the 2D-plane stress elastic quadratic element PLANE82 with mid-side nodes. Since the displacement field for a surface acoustic mode is only near the surface (in $0 < z < p$) we mesh this region of substrate finely and consistent with meshing of grating line. A coarse mesh is adopted for the bulk of the substrate as shown in Fig 4.2. The material properties used for the simulation are also shown in the figure. A fixed boundary condition is applied to the bottom of the substrate. A periodic Bloch condition $u_1 = u_2 exp(-ikp)$ ($u_1 = u_2$ for $k = 2\pi/p$) is applied on the vertical walls using constraint equations. The frequencies of the system in

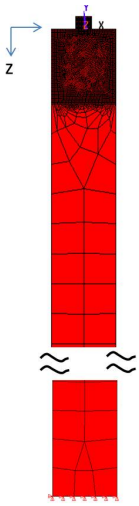

	E (GPa)	Poisson Rat	Dens (kg/m^3)
Substrate (Si)	130	0.27	2330
Grating (Al)	70	0.31	2700

Figure 4.2: Fine mesh at the surface.

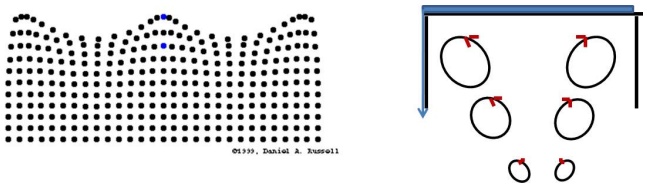

Figure 4.3: The displacement pattern of a Rayleigh mode.

the neighbourhood of SAW are extracted using Block-Lanczos scheme.

After the mode extraction, the displacement field of each mode is examined to characterize which one is the Rayleigh kind surface mode. The Rayleigh wave is a result of interaction of longitudinal and shear wave at the surface. Its amplitude decays along the depth exponentially as shown in Fig 4.3. Each particle in the mode has an elliptical path with ellipsity defined by longitudinal and shear velocities in the medium. The true Rayleigh waves only occur at a homogenous free surface. The simulation for free silicon yields a Rayleigh mode at $\nu = 12.26$ GHz for 400 nm periodicity. The Rayleigh wave displacements fields are shown in the Fig 4.4. The modal displacement fields clearly show that the surface energy is concentrated near the surface and the vector plot confirms that the observed mode was a Rayleigh mode.

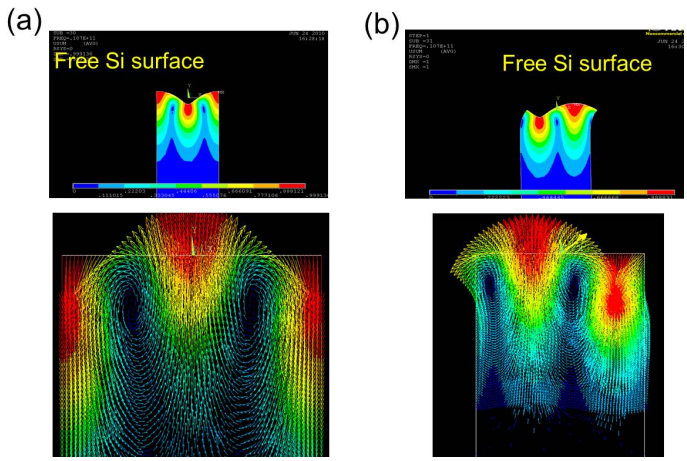

Figure 4.4: Rayleigh mode on free Si surface with two polarizations (a) and (b).

4.2 Analysis of surface modes with duty cycle

In this section, we discuss the frequency of the Rayleigh like mode for different duty cycles. The modal displacement at this frequency is also examined to judge the excitability of the mode. For the sake of discussion, four duty cycle regimes are defined - region I ($\eta = 0.1-0.25$), region II ($\eta = 0.3-0.55$), region III ($\eta = 0.6 - 0.75$) and region IV ($\eta = 0.80 - 0.95$).

In the high duty cycle regime, the gaps between the wide Al lines serve as the perturbation to the propagating SAW. The modal displacements of the dominantly mode (which has highest surface displacement that decays with the depth within $0 < z < p$) is shown in Fig 4.5. It can be seen that there is no displacement in the bulk of the substrate ($p < z < L$) suggesting that there is no coupling of SAW with the bulk. As a result of this, the surface acoustic wave has high quality factor. The frequency of the SAW mode with duty cycle in this regime follows a downward linear shift.

Two different polarizations of SAW modes designated as 'sin' like and 'cosine' like modes occur which have $u_x = 0$ at the faces 1 and 2 shown in Fig 4.1. In addition to these polarizations, another polarization where x-displacement of the vertical walls is dominant also occurs. The 'sin' like modes are lower in frequency compared to 'cos' like modes. In the unperturbed condition

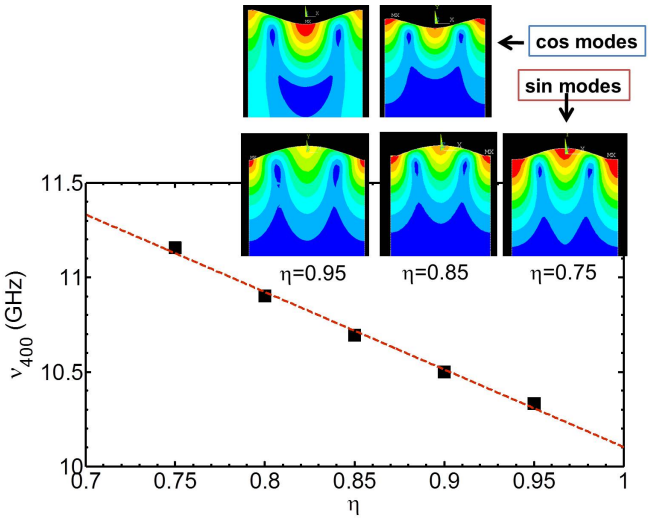

Figure 4.5: In the high duty cycle regime, $\Delta\nu$ follows a linear downward shift. The displacement fields show that energy is only concentrated near the surface.

(η=0 or η=1), these two modes are degenerate. There is a transition point frequency (TPF) at which there is a transition from 'sin' like to 'cos' like modes. In the region III, a 'sin' like mode with a frequency well below TPF is excited. The displacement field of the dominantly excited mode in this region show a slight coupling of the SAW modes with the bulk suggesting that the SAW generation efficiency is not as good that in the region IV. In this region, the frequency trend ceases to be linear.

In region II, the both 'sin' like and 'cosine' like modes at the TPF have similar probability of excitation and are dominantly excited modes. The corresponding displacement fields of these modes is shown in Fig 4.6. The displacement fields clearly show a significant coupling of SAW with the bulk modes. Both 'sin' and 'cosine' modes are equally dissipative (the radiation of energy from SAW to the bulk due to this coupling) and thus this region is unsuitable for SAW excitation. The frequency of the dominantly excited modes shown in Fig 4.6 with the duty cycle suprisingly has a positive slope. This is an unexpected trend as the increase in duty cycle corresponds to higher mass loading from the grating which should shift the frequency of SAW downwards if the Rayleigh velocity in the grating (V_R =3400 m/s in Al) is less than that in substrate (V_R =4910 m/s in Si). The observed trend

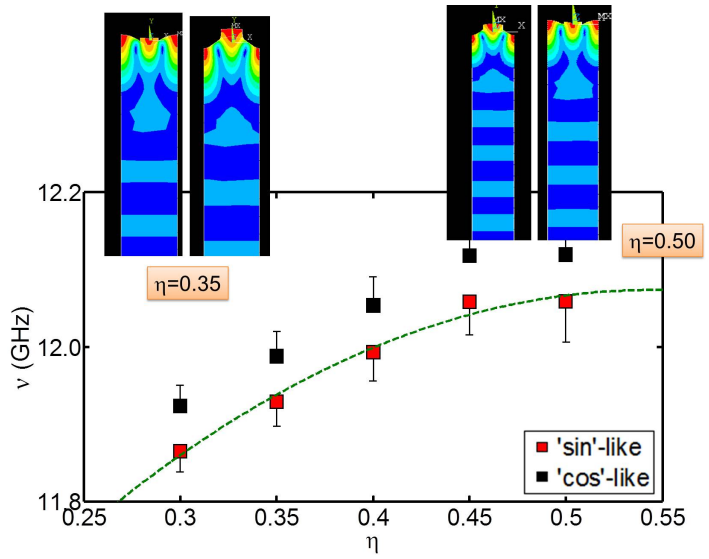

Figure 4.6: In this regime, $\Delta\nu$ follows sinusoidal trend and shows highest deviation from perturbation theory. The displacement fields show significant coupling of surface modes with the bulk.

is due to the reflection coefficient contribution to the frequency shift.

Finally, in the low duty cycle regime, the 'sin' like mode has displacement field with surface energy concentrated at the surface while 'cos' like mode is highly dissipative with excessive coupling of SAW with the bulk as seen in Fig 4.7. Thus 'sin' like mode at TPF is the dominantly excited mode. Due to a close resemblance of dominant excited mode to the true Rayleigh like mode, this duty cycle regime is very suitable for SAW generation.

In summary, the frequency of dominantly excited modes from the simulation at various duty cycle is shown in Fig 4.8. The trend is non linear with two inflexion points at $\eta = 0.25$ and $\eta = 0.50$ and a positive slope between these points. The prediction of the perturbation theory is close to the results from full eigenmode analysis of the composite in $\eta < 0.15$ and $\eta > 0.9$. The experimental results for frequency of SAW mode for p=400 nm gratings show excellent agreement with the full eigen analysis results. This excellent agreement proves the origin of photoexcited SAW generation in these periodic composites [19]. The thermal expansion of Al strongly couples to the substrate underneath which causes the surface acoustic wave. The deviation between the prediction of the eigen analysis and the perturbation theory is

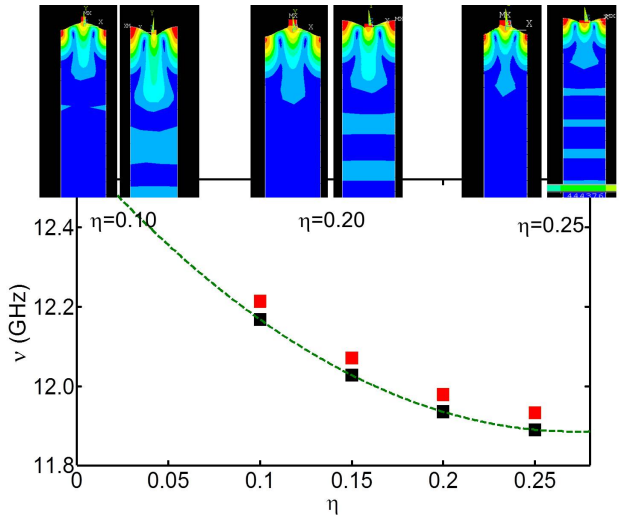

Figure 4.7: In this regime, $\Delta\nu$ becomes more linear and creeps towards perturbation theory below $\eta = 0.2$.

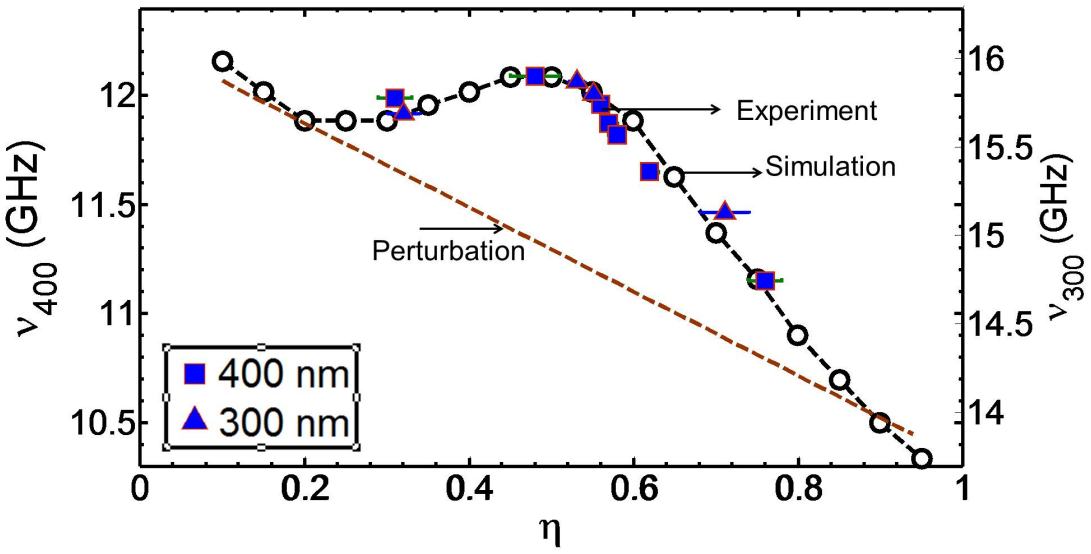

Figure 4.8: The frequencies obtained by full eigenmode analysis have excellent agreement with experiment for 300 nm and 400 nm gratings.

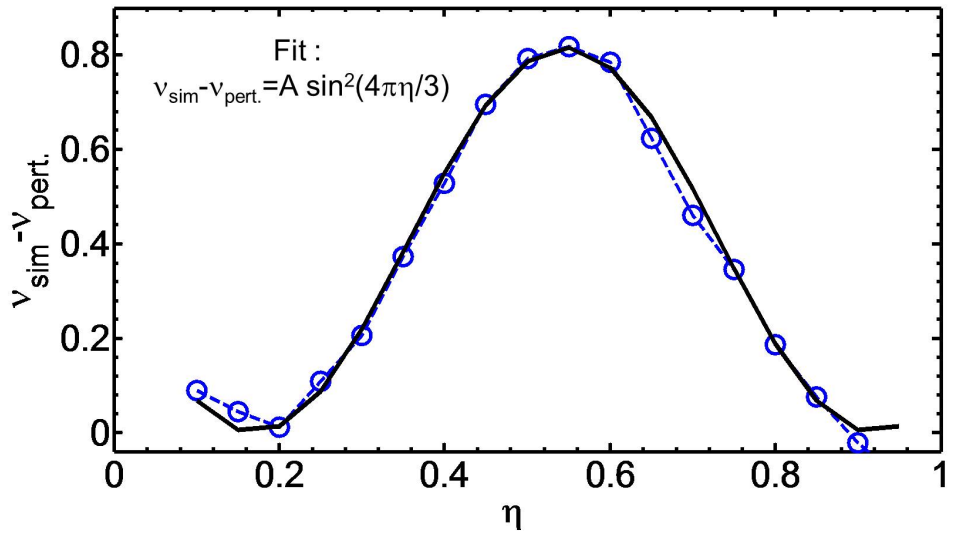

Figure 4.9: (a) The frequencies obtained by full eigenmode analysis have excellent agreement with experiment for 300 nm and 400 nm gratings.

shown in Fig 4.9. The deviation can be fitted by a curve of form $Asin^2(\pi\eta)$ as shown in the figure.

4.3 Attenuation with the duty cycle

Attenuation of the dominantly excited mode depends on the surface energy distribution in the neighbouring modes. A broadband excitation of the frequencies implies that the mode at the peak frequency is highly attenuated. In fact, for a second order damped system, the power function with frequencies is Lorentzian and the full width half maximum (FWHM) around the peak frequencies yields the attenuation coefficient of the frequency. With this idea in mind, we define a factor E_{distr} which is the ratio of strain energy in near the surface ($-h_{Al} < z < p$) to the sum of strain energy in the bulk ($p < z < L$) and near the surface. The mode with the highest E_{distr} is the dominantly excited mode. The FWHM of the E_{distr} spectrum around the dominant mode gives the attenuation of SAW.

There are two major extrinstic mechanisms for attenuation (γ) of SAW

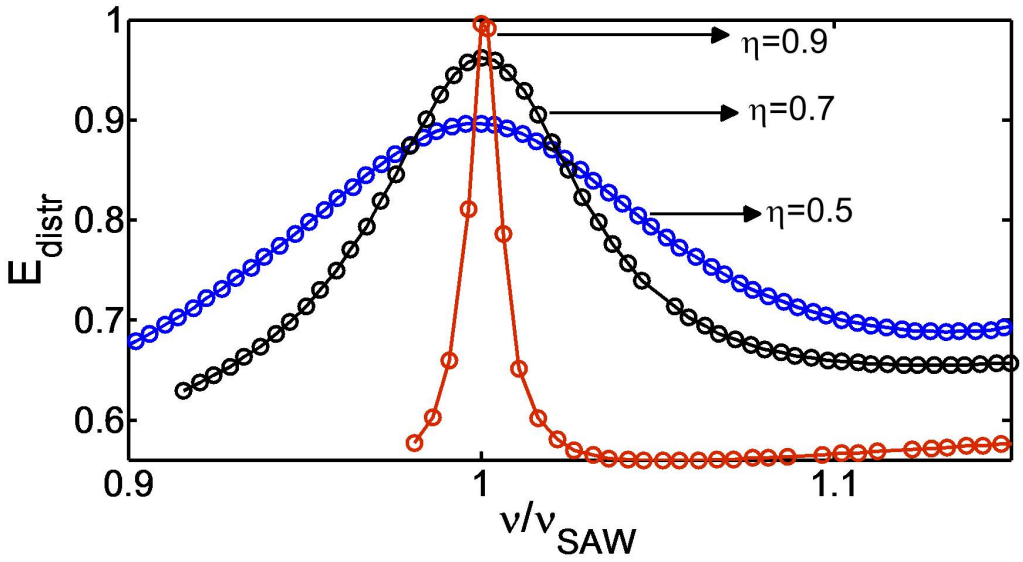

Figure 4.10: (a) The spread of E_{distr} around peak frequency increases from $\eta = 0.9$ to $\eta = 0.7$.

in this architecture. The first mechanism is the transfer of mechanical energy from the surface waves to the bulk due to the mass loading from the metal. The second mechanism is the spreading of mechanical energy from the confined excitation area, termed as phonon "walk-off". Secondary mechanisms include thermoelastic damping due to heat conduction across the film-substrate interface, Akheiser damping and the viscosity of the electron gas, all of which are shown to be only 5-10% of the observed damping[14]. Since the phonon walk-off effect does not change with the geometry of Al lines under same period of grating, we can rule out this mechanism. The dependence of γ with duty cycle then must be dominated by the radiation of SAW energy into the bulk.

The spectrum of E_{distr} for three different cycles in 300 nm grating periods is shown in Fig 4.10. The x-axis of the plot has frequency normalized by the peak frequency. It can seen that there is a broadband excitation of surface modes at η =0.5 suggesting highest attenuation of that particular mode at this frequency. The SAW generated at η =0.9 has very less attenuation. This effect translates into the factor called quality factor which is the ratio of the peak frequency and the FWHM spread of the E_{distr}. We thus conclude that

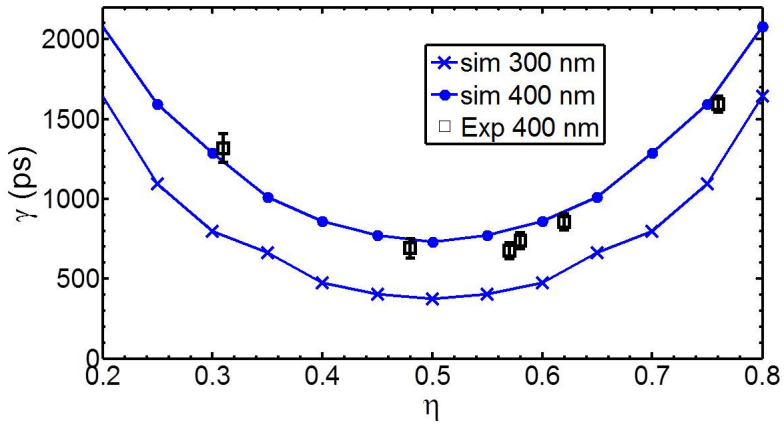

Figure 4.11: (a) The lifetime of surface oscillations predicted by eigenmode analysis for 300 nm and 400 nm has good match with experimental data.

quality factor of the SAW deteriorates at η =0.5.

This procedure is carried out for different duty cycles for 300 nm and 400 nm gratings and the inverse of FWHM in each case is plotted in Fig 4.11. We observe that the attenuation is maximum at $\eta = 0.5$ similar to the deviation in frequency of SAW from perturbation theory. This shows that there is a maximum coupling of surface modes with the bulk and thus highest energy is leaked out from surface vibrations into the bulk. This finding also complies with the modal displacement fields of the dominantly excited mode at $\eta = 0.5$ where the bulk longitudinal wave can be observed. This study thus gives insight into the scattering of surface acoustic waves from the periodic overlay which results in the attenuation.

According to the perturbation theory, the power density radiated out of the surface modes into the bulk is given by $P_z = AC\omega^4$ where A is area of interface between Al and Si, ω is the frequency of the wave, C is a constant depending on elastic properties of the grating and the substrate and is given by $C = (\rho_{Al}^2 h_{Al}^2 u_{z0}^2)\omega^4/(\rho_{Si} v_{l,Si})$. This theory predicts that the attenuation should linearly increase with the coverage area till $\eta < 0.5$ and then decrease linearly till $\eta = 1$. But this relation is only satisfied at low duty cycle and high duty cycle limits defined above. For the pseudosurface waves we observe in $\eta = 0.3 - 0.7$, there is a high deviation from the pertubation theory. The

eigenmode simulations results agree well with the experimental results.

In conclusion, the experimental results are successfully explained for full eignemode simulation of the periodic composite. This treatment departs from the perturbation theory in which the Al line is only considered as a small perturbation as seen by the propagating SAW which is clearly violated for high frequency SAW due to significant coupling with the bulk modes of Si. The dut cycle regimes $\eta > 0.8$ and $\eta < 0.2$ are suitable for sensing applications as the coupling of SAW with bulk is minimum in these dut cycle regimes. But in the duty cycle regime $\eta = 0.3 - 0.6$, the significant coupling renders SAW with a poor quality factor and thus insensitive to changes in the surface composition. The frequency shift predicted by the theory presented in this chapter deviates from the perturbation theory by $sin^2(\pi\eta)$ with highest deviation at $\eta = 0.5$. Similar conclusions in the attenuation analysis thus places significant limit on the duty cycle to be used for high frequency phononic crystals. Duty cycles in region I and IV are difficult to fabricate as sub-50 nm lines are required for SAW with $\nu > 20$ GHz.

CHAPTER 5

SUMMARY AND CONCLUSIONS

The generation and the detection of high frequency coherent surface acoustic waves of frequencies $\nu > 50$ GHz is scientifically significant for acoustic based metrology of nanostructures, chemical and bio sensors, ultrafast communications, microfluidics and spectroscopy. In addition, high frequency surface phonons in GHz regime (frequency close to phonons that contribute to heat transport) can be used to study ultrafast phonon mediated physical processes including heat transport and electron transport.

Generation of photoinduced thermal strain gradients in a periodic composite structure with nanometer scale gratings fabricated on a substrate is an attractive way of generating high frequency SAW. This is because the frequency of SAW excited in this process is inversely proportional to the period of the grating and thus the frequency is controlled by the state of art nanolithographic techniques. In the technique, ultrashort pulse laser is incident on a nanostructure grating on a substrate is differentially absorbed in grating and substrate. This in turn sets up a periodic thermal strain at the surface of the composite. This periodic thermal stress launches a surface acoustic wave with the same frequency as that of the grating period. Upon the analysis of the spectrum of SAW on the surface of substrate, the critical parameters that affect the frequency of SAW have been determined. A simple analysis shows that in order to achieve surface waves in $100-300$ GHz range, femtosecond laser pulses incident on the grating structure on the substrate should have a period less than 50 nm. In addition to this, it is desirable to have a substrate with high Rayleigh velocity, good optical absorption and low thermal conductivity. But at such frequencies, the effect of nanograting on the propagating SAW suppresses the efficiency of SAW generation. We thus study the effects of duty cycle and the period of nanograting on the attenuation of SAW.

We conducted experimental study of Al grating on Si substrate with duty cycles of Al grating varing from 20% to 80% and periods 300 nm and 400 nm. We demonstrated the picosecond ultrasonics technique for analyzing acoustics in hypersonic regime by probing for strain induced reflectivity change of the structure. The acoustic data was obtained by removing the thermal background from the time resolved reflectivity signals. We proved that the observed oscillations in the signals correspond to surface acoustic wave and has inverse dependence with the period of the grating. We analyzed the surface acoustic wave dynamics in Al-on-Si structure with varying duty cycle of the Al grating. We observed that the frequency shift ($\Delta\nu$) with increasing duty cycle is non linear instead of linear downward shift predicted by perturbation theory and maximum deviation occurs at $\eta = 0.5$. This led to the conclusion that the effect of Al grating on the high frequency SAW ($\nu >$10 GHz) is too significant to be predicted by perturbation theory. A similar conclusion to the $\Delta\nu$ was made regarding attenuation of SAW being that the attenuation of the wave is maximum around duty cycle $\eta = 0.5$.

The experimental results were explained by full eigenmode analysis of Si-Al composite structure and we show good agreement of the simulation results. This treatment departs from the perturbation theory in which the Al line is only considered as a small perturbation as seen by the propagating SAW which is clearly voilated for high frequency SAW due to significant coupling with the bulk modes of Si. The dut cycle regimes $\eta > 0.8$ and $\eta < 0.2$ are suitable for sensing applications as the coupling of SAW with bulk is minimum in these dut cycle regimes. But in the duty cycle regime $\eta = 0.3 - 0.6$, the significant coupling renders SAW with a poor quality factor and thus insensitive to changes in the surface composition. The frequency shift predicted by the theory presented in this chapter deviates from the perturbation theory by $sin^2(\pi\eta)$ with highest deviation at $\eta = 0.5$. Similar conclusions in the attenuation analysis thus places significant limit on the duty cycle to be used for high frequency phononic crystals. Duty cycles in region I and IV are difficult to fabricate as sub-50 nm lines are required for SAW with $\nu > 20$ GHz. The results of the work are summarized in Fig 5.1 and Fig 5.2.

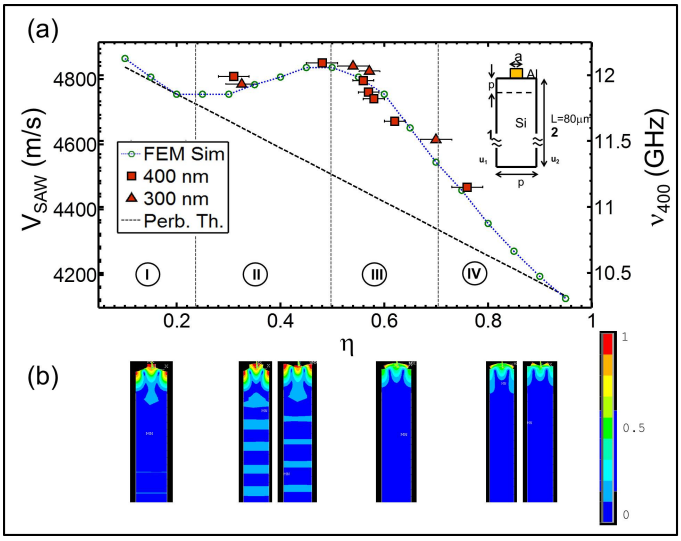

Figure 5.1: (a) The experimental SAW velocity shift (on left) and the frequencies of excited surface waves for $p = 400$ nm (on right) show good agreement with the results obtained by eigenmode analysis of the unit cell of the structure (shown in inset). The thin film perturbation theory is only valid for $\eta < 0.2$ (region (I)). (b) The displacement fields of the excited mode in different duty cycle regimes show highest coupling of surface modes with bulk modes in region (II).

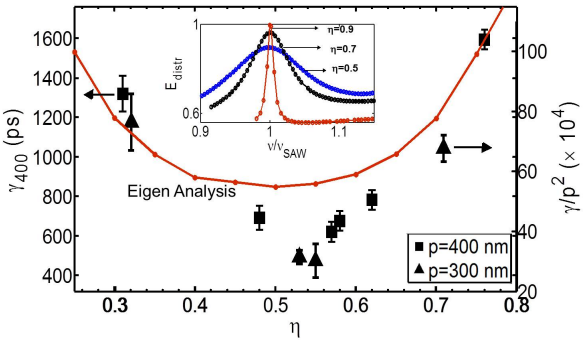

Figure 5.2: The damping time (γ) of surface acoustic waves in $p = 400$ nm is shown on the right of axis at corresponding cycles (square dots). The plot of damping time normalized by square of period (on left) as a function of duty cycle shows the highest attenuation in region(II). The damping time obtained by taking inverse of FWHM of surface energy spread ($0 < z < p$) around SAW mode is also shown.

REFERENCES

[1] I. Hosako and N. Sekine, "At the dawn of new era of terahertz technology," *Proc. of IEEE*, vol. 95, 2007.

[2] M. Tonouchi, "Cutting edge terahertz technology," *Nature Photonics*, vol. 1, pp. 97–105, 2007.

[3] M. Nagel, M. Forst, and H. Kurz, "Thz biosensing devices: fundamentals and technology," *J. Phys, Condens. Matter*, vol. 18, pp. 601–618, 2006.

[4] S. Capinski and H. Maris, "Improved apparatus for picosecond pump-probe measurements," *Rev. Sci. Instrum*, vol. 67, p. 2720, 1996.

[5] T. Lee and G. Cahill, "Elastic constants of single-crystal tin(001) by picoseconds ultrasonic measurements," *Phys.Rev. B*, vol. 71, p. 144106, 2005.

[6] C. Thomsen, H. T. Grahn, H. J. Maris, and J. Tauc, "Surface generation and detection of phonons by picosecond light pulses," *Phys.Rev.B*, vol. 34, p. 4129, 1986.

[7] J. A. Rogers, A. A. Maznev, M. J. Banet, and K. A. Nelson, "Optical generation and charaterization of acoustic waves in thin films," *Annu. Rev. Mater. Sci.*, vol. 20, pp. 117–157, 2000.

[8] D. H. Hurley, R. Lewis, O. Wright, and O. Mastuda, "Coherent control of gigahertz surface acoustic and bulk phonons using ultrafast optical pulses," *Appl. Phys. Lett.*, vol. 93, p. 113101, 2008.

[9] A. Kolomenskii and A. Maznev, "Observation of phonon focusing with pulsed laser excitation of surface acoustic waves in silicon," *JETP Lett.*, vol. 53, p. 8, 1991.

[10] Talyanskii, J. Shilton, D. Ritchie, and G. Jones, "Single-electron transport in a one-dimensional channel by high-frequency surface acoustic waves," *Phys. Rev.B*, vol. 56, p. 15180, 1997.

[11] B. Bonello, B. Perrin, E. Romatet, and J. C. Jeanet, "Application of the picosecond ultrasonic technique to the study of elastic and time-resolved thermal properties of materials," *Ultrasonics*, vol. 35, pp. 223–231, 1997.

[12] M. Seimens, Q. Li, R. Yang, K. Nelson, H. Anderson, M. Murnane, and C. Kapteyn, "Quasi-ballistic thermal transport from nanoscale interfaces observed using ultrafast coherent soft x-ray beams," *Nature Mat.*, vol. 9, pp. 26–30, 2010.

[13] M. E. Seimens, Q. Li, M. M. Murnane, H. C. Kapteyn, R. Yang, E. H. Anderson, and K. A. Nelson, "High-frequency surface acoustic wave propagation in nanostructures characterized by coherent extreme ultraviolet beams," *Appl. Phys. Lett.*, vol. 94, p. 093103, 2009.

[14] H. N. Lin, H. J. Maris, L. B. Freund, K. Y. Lee, H. Luhn, and D. P. Kern, "Study of vibrational modes in gold nanostructures," *J. Appl. Phys.*, vol. 73, p. 37, 1993.

[15] B. Bonello, A. Ajinou, V. Richard, P. Djemia, and S. M. Cherif, "Surface acoustic waves in the ghz range generated by periodically patterned metallic stripes illuminated by an ultrashort laser pulse," *J. Acoust. Soc. Am.*, vol. 110, p. 4, 2001.

[16] D. H. Hurley and K. L. Telschow, "Picosecond surface acoustic waves using suboptical wavelength absorption grating," *Phys. Rev. B*, vol. 66, p. 153301, 2002.

[17] J. R. Friend, L. Y. Yeo, D. R. Arifin, and A. Mechler, "Evaporative self-assembly assisted synthesis of polymer nanoparticles by surface acoustic wave atomization," *Nanotechnology*, vol. 19, p. 144106, 2008.

[18] B. A. Auld, *Acoustic Fields and Waves in Solids*. Malabar, FL: Krieger Publ., 1990.

[19] C. Giannetti, B. Revaz, F. Banfi, M. Montagnese, G. Ferrini, F. Cilento, S. Maccalli, P. Vavassori, G. Oliviero, E. Bontempi, L. E. Depero, V. Metlushko, and F. Parmigiani, "Thermomechanical behavior of surface acoustic waves in ordered arrays of nanodisks studied by near-infrared pump-probe diffraction experiments," *Phys. Rev. B*, vol. 76, p. 125413, 2007.

[20] A. Neubrand and P. Hess, "Laser generation and detection of surface acoustic waves: Elastic properties of surface layers," *J. Appl. Phys.*, vol. 71, p. 1, 1992.

[21] A. A. Karabutov, "Laser excitation of surface acoustic waves: a new direction in opto-acoustic spectroscopy of a solid," *Sov. Phys. Usp.*, vol. 28, p. 11, 1985.

[22] D. Nardi, F. Banfi, C. Giannetti, B. Revaz, G. Ferrini, and F. Parmigiani, "Pseudosurface acoustic waves in hypersonic surface phononic crystals," *Phys. Rev. B*, vol. 80, p. 104119, 2009.

[23] S. Datta and B. J. Hunsinger, "First-order reflection coefficient of surface acoustic waves from thin-strip overlays," *J. Appl. Phys.*, vol. 50, p. 9, 1979.